MSc in Climate Change

Linking Large Scale Atmospheric Modes of Variability with Fluctuations in the Atlantic Ocean

Andrea Vang

Supervised by Jens Hesselbjerg Christensen, Bogi Hansen and Karin Margreta H. Larsen

May 2023

Andrea Vang

Linking Large Scale Atmospheric Modes of Variability with Fluctuations in the Atlantic Ocean

MSc in Climate Change, May 2023

Supervisors: Jens Hesselbjerg Christensen , Bogi Hansen and Karin Margreta H. Larsen

University of Copenhagen

Faculty of science

Masters Degree in Climate Change

Tagensvej 16A

2200 Copenhagen N
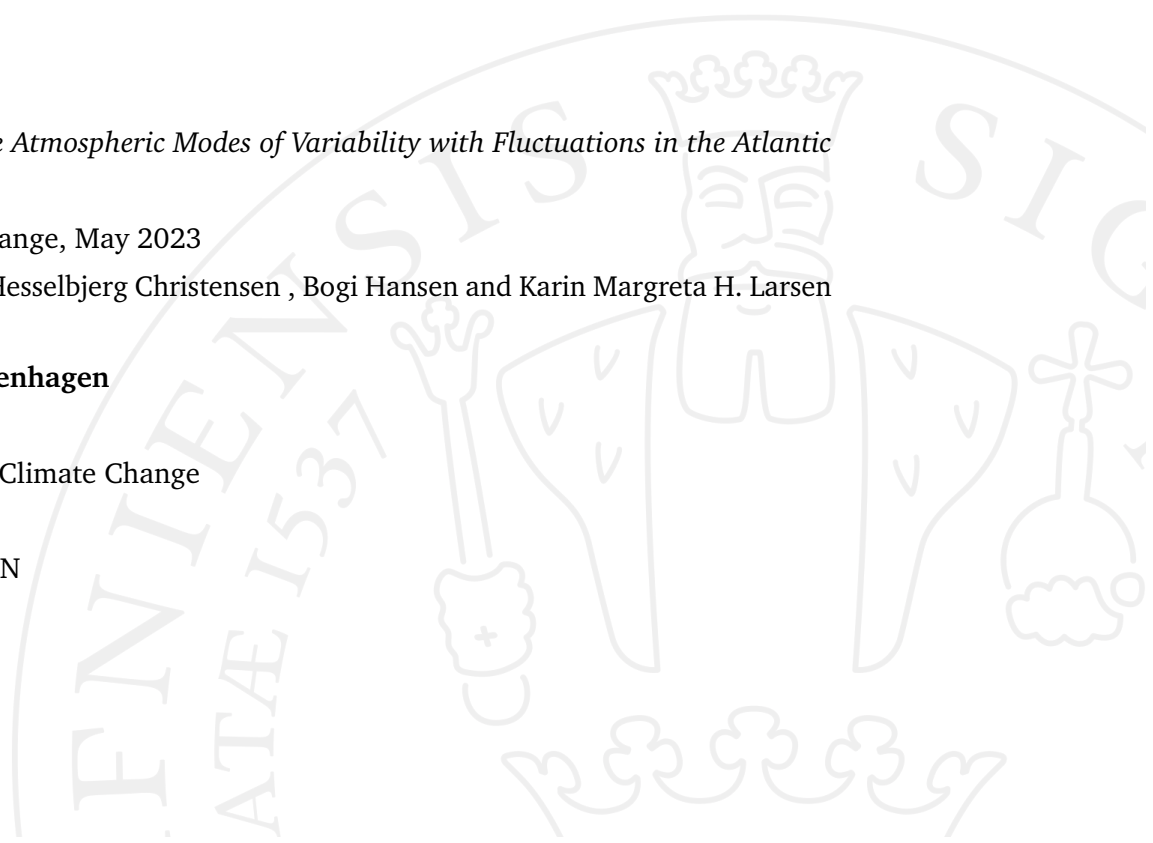
Abstract

This thesis successfully performed an EOF analysis on MSLP, SST, OHC, Salinity and Current speed, identifying the leading modes of variability. PC time series were used to determine which patterns of variability co-varied with NAO, as well as determining a lag on monthly time scales between the oceanic variables and NAO. A PC regression analysis was performed, where the oceanic variables were regressed onto the NAO. The results from the PC time series comparisons and the PC regressions proved that the SST tripole pattern is closely linked to the NAO and lags the NAO by one month on shorter timescales. This link can also be seen in the OHC with the same time lag. The NAO and SSH were also shown to be closely linked with no time lag. Especially in the North and Baltic Sea, the SSH was strongly positively correlated with the NAO. The zonal current speed was found to be strongly correlated to the NAO around Scandinavia and across the GSR. However, the regression coefficients was not very strong in most places.

Observational data of ocean currents across the GSR and Skagerrak was investigated, to determine if they were affected by NAO index. They were plotted against NAO index, and a linear trend was fitted. The observational data from the FSC volume transport showed a small positive trend with NAO index. The other two currents, NIIC and the IF current, did not show an influence from the NAO. The observational data from Skagerrak showed a small westward trend with NAO index. This was due to the counter current positioned north of the strong eastward current that arose with NAO.

Acknowledgements

Contents

List of Abbreviations

AMO - Atlantic Mulitdecadal Oscillation

AMOC - Atlantic Meridional Overturning Circulation

EOF - Empirical Orthogonal Function

GSR - Greenland-Scotland Ridge

MOC - Meridional Overturning Circulation

MSLP - Mean Sea Level Pressure

NA - North Atlantic

NAO - North Atlantic Oscillation

OHC - Ocean Heat Content

PC - Principal Component

SST - Sea Surface Temperature

SSH - Sea Surface Height

Introduction

Understanding the mechanisms that drive the variations observed in the climate is vital in combating the nature crisis humanity is currently facing. Climate variability is an integral part of the Earth system - however, the drastic changes that are currently being observed are unprecedented. Therefore, it is of great importance that we gain more knowledge on how to forecast climate events that can influence our lives. This project aims to research the connections between atmospheric modes of variability over the North Atlantic to the variability in the North Atlantic Ocean. This plays into the project 'GreenPlanning', which aims to better the understanding of the predictability of the modes of variability in the atmosphere in the North Atlantic, specifically the North Atlantic Oscillation (NAO) , which are known to affect the weather in Europe.

This thesis aims to answer the questions:

- How does the North Atlantic Oscillation influence oceanic variables in the North Atlantic?
- Is it possible to identify a time lag between North Atlantic Oscillation phases and oceanic variables?
- Is it possible to see an effect of the North Atlantic Oscillation in oceanic observational data?

The thesis will look into how the North Atlantic Oscillation influences the oceanic variables Sea Surface Temperature, Heat Content, Sea Surface Height, Current Speed, and Salinity. This will be done with an Empirical Orthogonal Function Analysis and Principle Component Regression Analysis. The lag will be determined using cross correlation. Lastly, this thesis will look at observational data of volume transport over the Greenland-Scotland ridge, as well as data of the eastward current in Skagerrak from radar observations, to see if they are influenced by the North Atlantic Oscillation.

Background

<div style="text-align: right">2</div>

Understanding the connection between ocean and atmosphere circulation is vital in understanding the interactions of the Earth system. In order to better this understanding, this chapter explores the connection between the North Atlantic Oscillation (NAO) and circulation in the ocean, but first it will briefly dive into ocean and atmospheric circulation individually.

2.1 Atmospheric Circulation & The North Atlantic Oscillation

The circulation in the atmosphere is a chaotic system and challenging to predict. However, there are general patterns of circulation that are driven by the differences in incoming solar radiation at different latitudes. The highest incoming solar radiation is at the Equator, while the lowest is at the poles. This creates a temperature imbalance, which the general circulation system tries to resolve. The warm tropical air will want to flow northward while the cold polar air will want to flow south. A schematic of the general circulation can be seen in Figure 2.1 At the equator a low pressure is formed due to the warm buoyant air rising. The rising air starts travelling north at the tropopause. The air cools and is deflected to the right due to the Coriolis force. The deflection inhibits the northward flow, and the air circulates back down at around $30°$N, forming a high pressure. This induces a circulation cell known as the Hadley cell (Lutgens *et al.*, 1995).

Due to the air being relatively colder at the pole than at $60°$N, the air is denser at the pole and the troposphere is lower. This results in a high pressure situated at the pole and a relatively low pressure at $60°$N. This creates the circulation cell called the Polar cell (Lutgens *et al.*, 1995).
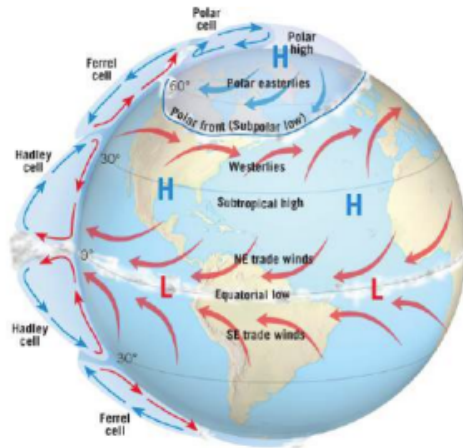
Figure 2.1: A depiction of the general circulation pattern in the atmosphere. The figure is taken from Lutgens *et al.*, 1995.

In the mid latitudes between the Hadley and Polar cell, you get a circulation cell that is basically driven by the other two, called the Ferrel cell. In each of these cells, air masses are travelling along the latitudes. These air masses experience the Coriolis force and are deflected to the right in the northern hemisphere. This induces north-easterly winds in the Hadley cell, westerly winds in the Ferrel cell and easterlies in the Polar cell (Lutgens *et al.*, 1995).

The conditions explained above would prevail if there were no perturbations in the circulation system, but this is very much not the case. However, this general circulation pattern does tell us something about how the mean weather conditions are. The mean state of the weather system over the area of interest for this thesis can be seen in Figure 2.2.
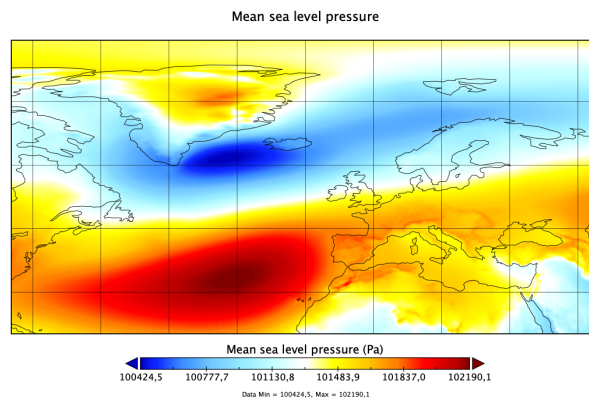
Figure 2.2: The mean state of the pressure system at sea level over the NA region.

It can be seen that the mean state of the pressure in the NA has a high pressure at the subtropics followed by a low pressure at around $60°$N and a high pressure at the pole. This follows the general circulation pattern as explained above.

The atmospheric circulation system over the North Atlantic (NA) is largely dominated by the NAO, which largely resembles the mean field of sea level pressure in Figure 2.2 (Hurrell *et al.*, 2003). The NAO has two distinct phases, a positive and a negative phase. The positive phase is characterized by a strong low pressure over Iceland and a strong high pressure over the Azores, the negative phase has weaker lows and highs, respectively (Hurrell *et al.*, 2003). This means that the NAO is actually an anomaly deviating from the pattern that can be seen in Figure 2.2. Whether the system is in a positive or negative phase has a large impact on the weather in the surrounding area.

The phases of NAO are illustrated in Figure 2.3. NAO is characterised by an index that is based on the normalized station-based pressure difference between Iceland and the Azores. It shows that a positive NAO results in wet and warm conditions in Scandinavia, dry conditions in the Mediterranean, intensified westerly trade winds, a stronger NA current, warming in the ocean at the mid latitude, and a cooling elsewhere (SST-tripole). When the NAO index is negative, conditions are dry in Scandinavia, wet in the Mediterranean, weaker westerlies, weaker NA current, and a reversed SST-tripole. It is common to express the NAO index as means of the winter months, which can be seen in Figure 2.4.

The higher pressure gradient between Iceland and the Azores that comes with a positive NAO, results in higher surface winds and an intensified westerly storm-track with a slight northward shift. This affects the wind driven currents in the ocean, and, as can be seen on Figure 2.3, the Gulf stream and NA current are also intensified (Taylor and Stephens, 1998). The effects of positive/negative NAO on ocean circulation will be discussed further in Section 2.3.

2.2 Ocean Circulation

This section will look into the general ocean circulation in the Atlantic region to better understand the different components in the system. The Atlantic
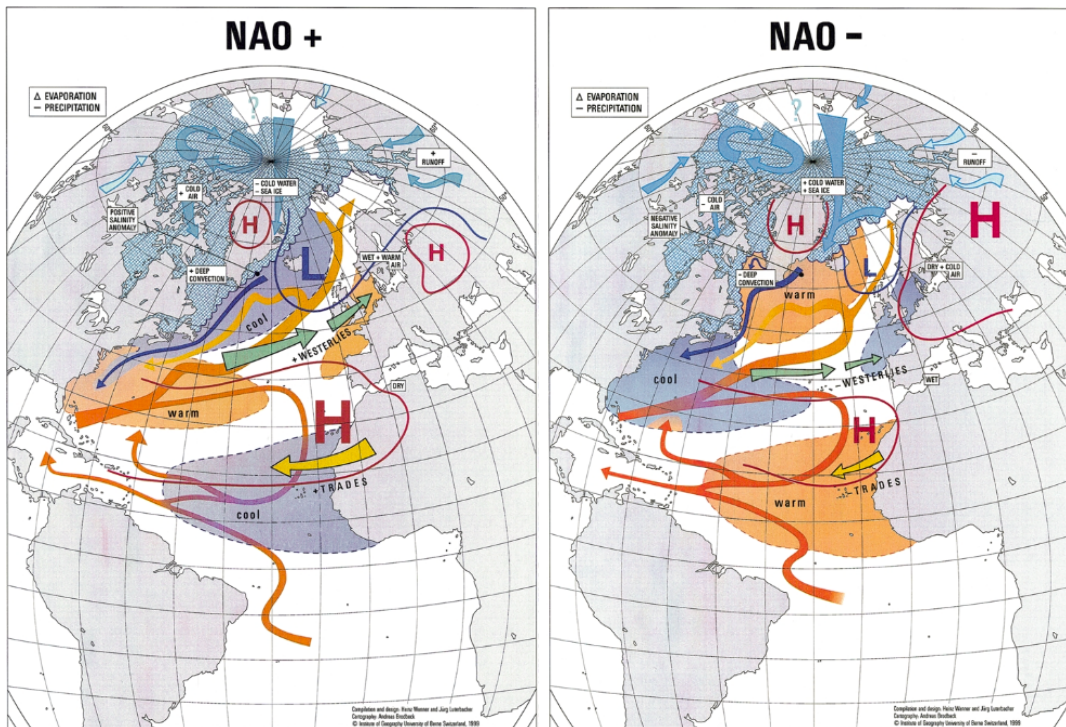
Figure 2.3: The two phases of the NAO. To the left, the positive phase, there are wet and warm conditions in Scandinavia, dry conditions in the Mediterranean, intensified westerly trade winds, a stronger NA current, warming in the ocean at the mid latitude, and a cooling elsewhere (SST-tripole). To the right, the negative phase, where conditions are dry in Scandinavia and wet in the Mediterranean, weaker westerlies and weaker NA current and a reversed SST-tripole. This illustration is taken from Wanner *et al.*, 2001.

Meridional Overturning Circulation (AMOC) is a system of ocean currents driven by many different mechanisms. The main mechanisms driving the AMOC are differences in temperature and salinity between the tropics and the arctic. The components of the AMOC in the NA ocean can be seen on Figure 2.5. Water travelling north with the Gulf stream is split into two, where some of the warm water is recirculated in the sub tropical circulation cell, and some water circulates north in the subpolar cell. As the water moves towards the Arctic, its salinity tends to decrease due to net precipitation and mixing with low-salinity waters. This acts towards decreasing the surface density, while at the same time the water loses heat to the atmosphere. The cooling dominates the freshening so that the density of the surface waters generally increases. Eventually, the water becomes so dense that it sinks and makes its way south again. This is called overturning circulation, which mainly occurs in the Nordic Seas and in the Labrador Sea.
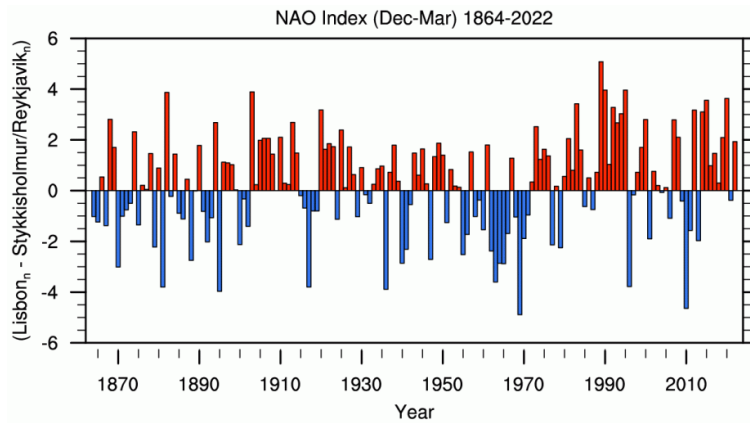
Figure 2.4: The NAO index of the winter mean, based on the pressure difference between Lisbon and Stykkishólmur/Reykjavík. The figure is taken from Hurrell and Atmospheric Research Staff, 2021.

This mechanism is vital in driving the AMOC. It is well established that the AMOC has slowed down and even collapsed before, leading to abrupt climate change. During a warmer climate, the freshwater input into the Arctic and NA waters increases due to ice sheet and glacier melt and less sea ice formation, ultimately lowering the salinity. The warmer climate also results in less cooling as water moves north. These effects combined result in a slowing overturning circulation, since the water travelling north does not become as dense. Sometimes this can halt the circulation all together.

Since the AMOC acts as a heat conveyor to the northern hemisphere, the slowing or halting of the overturning circulation will cool the northern hemisphere. This cooling will then, in turn, cause less freshwater input into the Arctic and NA ocean, making the overturning stronger again. Therefore, this is a negative feedback loop and a self regulating system.

This self regulating mechanism is also referred to as the inter-hemispheric Atlantic seesaw. Since the AMOC is vital in distributing heat from the tropics to the Arctic, when it slows down, there will be an accumulation of heat in the Southern Atlantic, and vice versa when it speeds up. This results in a seesaw effect where heat oscillates back and fourth between the southern and northern hemisphere.

There are many other less dramatic variabilities on smaller timescales in the NA. The main mode of variability on decadal time scales is known as the Atlantic Multidecacdal Oscillation (AMO). The AMO is an oscillation in the
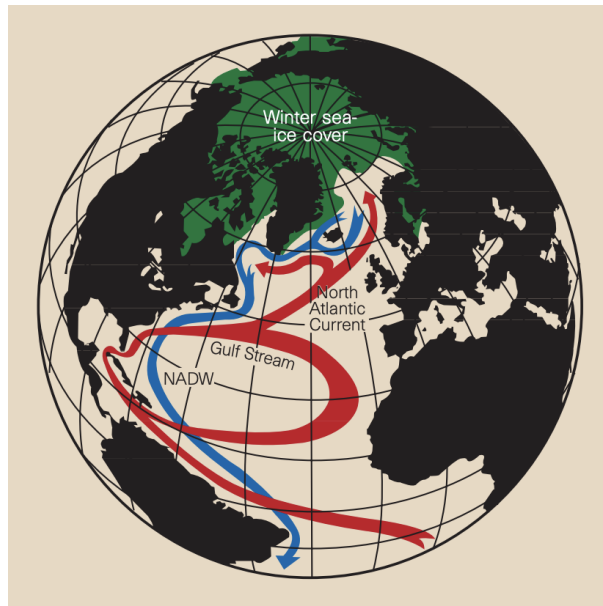
Figure 2.5: A depiction of the northern part of the AMOC. The figure is taken from Rahmstorf, 1997.

SST pattern in the NA region that has a period of 60-80 years. The AMO should be distinguished from the interannual variability related to the NAO. The AMO index is defined by the average of detrended NA SST anomalies. In order to reflect the low frequency variability in the Atlantic, the anomalies are also filtered through a 10 year low pass filter (Trenberth *et al.*, 2019). A time series of the AMO can be seen in Figure 2.6.
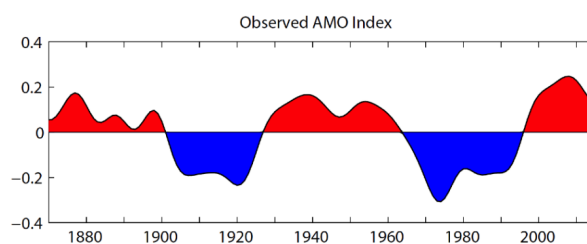
Figure 2.6: A time series of the AMO index. Positive AMO phases correspond to positive SST anomalies in the NA. The figure is taken from Trenberth *et al.*, 2019.

A positive AMO index refers to a uniformly positive temperature anomaly in the NA, which is thought to be driven by small changes in the AMOC. However, there are disputes as to whether this is the case, or if it is driven by changes in radiative forcing due to anthropogenic activity. Some studies suggest it is a mix of both (Trenberth *et al.*, 2019).

2.3 Interactions Between Atmospheric and Oceanic Circulation in the North Atlantic

The atmospheric and oceanic circulations are complex individually, but they have even more complex interactions. Since this thesis looks into NAO and the oceanic variables, only the interactions between NAO and the ocean will be discussed.

In general the ocean responds to the atmosphere on timescales shorter than a decade, where it might be the other way around on longer timescales (Hurrell and Visbeck, 2003). As mentioned before, the Gulf stream/NA Current is a wind driven current. Since NAO influences the strength and position of the westerly trade winds, it also affects the wind driven circulation in the ocean, including the Gulf stream. The wind stress induces Ekman transport, which has an effect on the circulation. The Ekman transport can be expressed as a function of wind stress like so,

$$M_{ek} = (-k \times \tau')/(\rho_0 * f). \tag{2.1}$$

Where k is a vertical unit vector, τ' is the wind stress anomaly, ρ_0 is a reference density and f is a Coriolis parameter (Hurrell and Visbeck, 2003). During positive NAO there is a pole-ward Ekman transport south of $40°$N and an equator-ward Ekman transport north of $40°$N, this arises due to the wind stress in the region, which can be seen in Figure 2.7.

These Ekman transports converge and must induce downwelling below the surface layer. Since there is no net meridional flow, this must be balanced by an equal and opposite flow beneath. This results in a contribution to the stream function of the meridional overturning circulation(MOC) with a maximum under the Ekman layer at around 300m (Hurrell and Visbeck, 2003). This effect on the Ekman transport also affects other oceanic variables.

When the NAO affects the Ekman part of the MOC, it is to be expected that it affects the poleward heat transport as well. Hurrell and Visbeck, 2003 perform a theoretical estimate on how much poleward heat transport the NAO results
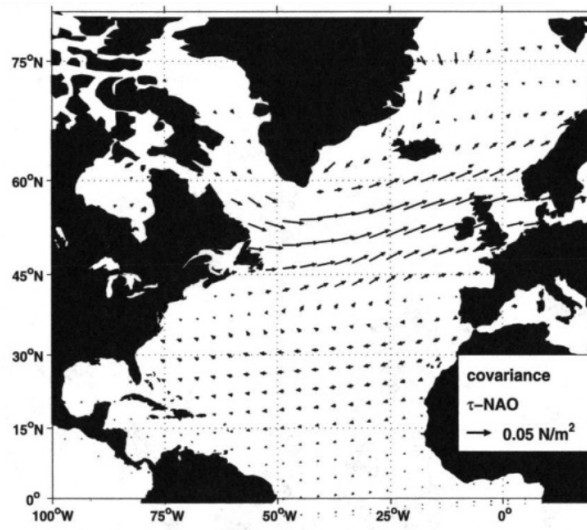
Figure 2.7: The co-variance of wind-stress and NAO index. The figure is taken from Hurrell and Visbeck, 2003.

in, taking into account Ekman transport, changes in the subtropical gyre and changes in the density field due to buoyancy loss and advection. They find that the poleward heat transport south of $45°$N would be enhanced by 0.05PW after weeks of persistent positive NAO. North of $50°$N, the poleward heat transport would decrease about 0.05PW. The subpolar gyre would offset the Ekman part of the MOC to a positive anomaly of 0.03PW (Hurrell and Visbeck, 2003). These changes in the heat distribution and circulation result in a characteristic SST tripole pattern, which is shown in 2.3. Studies have shown that, on top of this, the SST tripole pattern has a positive feedback with NAO, meaning that this system enhances itself (Pan, 2005).

Figure 2.8 shows a simplified schematic of how the NAO affects the AMOC. This figure specifically explores the change in the NAO phase where it was strongly positive before 1995, and more neutral and negative after 1995. It can be seen that the persistent NAO in (A) results in a Gulf stream that reaches further north, a stronger subtropical gyre and a weaker subpolar gyre. In Toma *et al.*, 2022, they also claim that the persistent positive NAO resulted in an increase in deep water formation, because a positive NAO results in colder waters around Greenland and in the Labrador sea. It can also be seen that during the "post-2000 circulation state", the Gulf stream is more horizontal and the subpolar gyre is stronger.
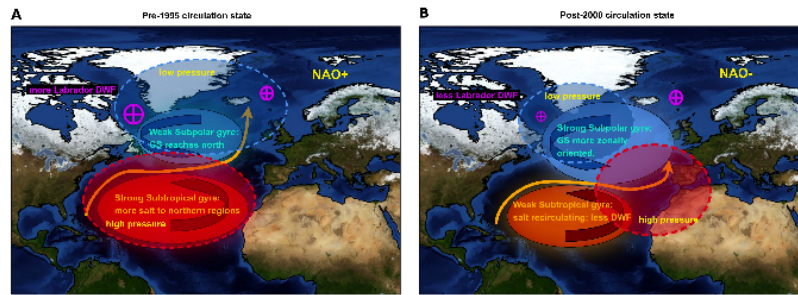
Figure 2.8: A schematic that shows the simplified effects of the NAO on the AMOC. In (A) you can see the high and low pressure associated with a strong positive NAO. A persistent NAO, like observed in the 1990s, will induce the SST tripole pattern, and influences the gyre circulation and the position of the Gulf stream. (B) shows how a negative/neutral NAO influences the position of the Gulf stream and the gyre circulation. The figure is taken from Toma *et al.*, 2022.

When it comes to observed changes in the ocean due to NAO, one of the most apparent ones is the sea surface height (SSH) anomalies. When the NAO is strongly positive, the SSH in the northern NA will decrease and the SSH will increase in the southern NA (Iglesias *et al.*, 2017) (Volkov and Aken, 2003).

This is due to the baroclinic transport becoming stronger (weaker) during positive (negative) NAO, which causes a strengthening (weakening) in the horizontal component of the thermohaline circulation in both the subpolar and subtropical gyres (Volkov and Aken, 2003). Weak westerlies associated with a negative NAO index also induces warming in the subpolar gyre, resulting in density decrease and a higher SSH (Volkov and Aken, 2003). It should be mentioned that the SSH response to pressure anomalies is very complex, because there are a lot of different components at play. For example, one would expect that a high pressure would result in a negative local SSH anomalies. Despite this, a positive NAO results in a lowering of the SSH under the atmospheric low center around Iceland and an increase in SSH under the atmospheric high. This means that the other components explained earlier have a stronger effect.

There are also clear correlations between the NAO and the SSH in the Baltic and the Mediterranean. Because of the intensified westerlies during a positive NAO, the water is "pushed" up against northern Europe and Scandinavia. This results in the SSH increasing in the Baltic sea (Iglesias *et al.*, 2017).

As made clear by this short introduction, the interactions between the NAO and the oceanic variables are manifold and very complicated. And this is precisely what this thesis will attempt to make an overview of. In the next section, it will be discussed how to do so.

Data and Methods

This chapter describes what data is used, how it is pre-processed, and what methods are used to analyse the data.

3.1 Data

The first section of this thesis uses reanalysis data downloaded from the Copernicus Climate Data Store, where the NAO signal in the data is analysed against different oceanic variables in order to estimate the effects of the NAO on the ocean. The second section of the thesis attempts to link observational data to the NAO index.

3.1.1 Reanalysis Data

Reanalysis data is climate models that run while being fed with observational data when available. This means that the model "fills in the blanks" where there is no observational data. Reanalysis data is widely used, because it is the best complete data of past weather that is currently possible to produce.

Two data sets were used; ERA5 and ORAS5. ERA5 is the fifth generation European Centre for Medium-Range Weather Forecasts (ECMWF) atmospheric reanalysis of the global climate covering the period from January 1950 to the present (C3S, 2023b). ORAS5 is the Ocean Reanalysis System 5, also made by ECMWF. It includes five ensemble members and runs from 1959 to the present (C3S, 2023a). Both of these data sets have a resolution of 0.25°x0.25° (25 km in the tropics and 9 km in the Arctic).

The variables downloaded from ERA5 was mean sea level pressure (MSLP) in Pascals and sea surface temperature (SST) in Kelvin. The variables downloaded from ORAS5 were ocean heat content (OHC) of the upper 300m (J m-2), Sea

Surface Height(SSH) (m), salinity (PSU), meridional current (m s-1), zonal current (m s-1), and sea ice thickness (m). All data was 2D except salinity, meridional and zonal currents, which were 3D since they included vertical levels of ocean depth. The time constraints of the data sets define the period of interest running from 1959 to present. The defined area of interest is -80°W, 20°E, 20°N and 90°N. The mean fields of the variables can be seen in the Appendix in Figure 8.1(notice that the mean field of MSLP has already been presented in the Background).

3.1.2 Preprocessing of Data

Most of the preprocessing of the reanalysis data was done using Climate Data Operators (CDO). It was made sure that all the variables had the same time resolution and spanned the same space (Schulzweida, 2022). These were heat content and SST, since these are directly linked to global warming. It should, however, be mentioned that heat content and SST were also analysed without detrending, in order to identify what difference this makes.

To achieve an expression for the total current speed, the meridional and zonal currents were combined using the operator using CDO. For the variables with vertical levels, salinity, and current speed, a weighted vertical mean was taken of the upper 300 m.

All of the data was deseasonalized by taking the monthly means of the individual months over the whole time series, and then subtracting this mean from each corresponding month in the time series. This is done for each gird point. This was done because in all cases, the main variability of the data is due to seasonal variation, which is not of interest in this thesis.

All of the oceanic variables were masked so to filter out the effects of sea ice. This was easier for some of the variables than for others. Especially salinity was greatly affected by sea ice variations. In the case of salinity, the Mediterranean and the Baltic sea were also masked out, due to their very high/low salinity concentrations when comparing to the rest of the Atlantic Ocean.

SST and OHC were detrended. The 'normal' way of detrending is finding the trend of the time series in each point and subtracting the trend from the

respective points. This way of detrending has some flaws tied to it as explained in Trenberth *et al.*, 2019. These flaws are specifically tied to detrending SST and OHC, because

- The success of the detrending depends on the length of the time series
- It assumes that the trend goes indefinitely into the past and future
- For SST and OHC, there was no global warming trend in the early part of the 20th century. There was actually a cooling trend.

Removing a global time series from each point instead of the local trend resolves these three issues with detrending (Trenberth *et al.*, 2019). The data was detrended using a global mean (in the area of interest) and subtracting that from each point in order to avoid the previously mentioned flaws.

3.1.3 Observational Data

Observational data from moorings around the Faroe Islands were used. The Faroe Marine Research Institute, Marine Scotland Science and others regularly deploy moorings in order to gather observations on the currents on the Ridge. They also synthesize the data into time series of volume and heat transport across the Greenland-Scotland ridge (GSR)[1]. The different sites where measurements are done are shown in Figure 3.1.

As it can be seen on Figure 3.1 the red arrows indicate surface currents with Atlantic water flowing into the Nordic Seas, and the blue arrows indicate the overturning currents of North Altantic Deep Water returning into the Atlantic from the Nordic Seas.

The overflowing currents are not of interest in this thesis, since they are not directly affected by atmospheric circulation. The surface currents indicated in red are affected by atmospheric circulation. Therefore the currents that will be considered are the North Icelandic Irminger Current, the Faroe Current and the Faroe-Shetland Channel inflow which are numbered 1, 2 and 3 on Figure 3.1.

---

[1]The Greenland-Scotland Ridge inflow time series are available at `http://www.oceansites.org/tma/gsr.html`. Time series update for the Faroe Current was provided by Karin Margretha H. Larsen, Faroe Marine Research Institute and for the Faroe-Shetland inflow by Barbara Berx, Marine Scotland Science.
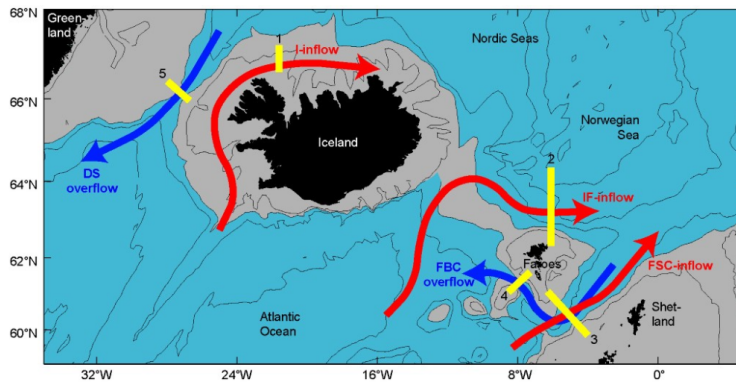
Figure 3.1: A map of the sites where measurements are made of the currents across the Greenland-Scotland ridge, marked with yellow lines. The currents are 1: North Icelandic Irminger Current (NIIC; I-inflow), 2: Faroe Current (IF-inflow), 3: Faroe-Shetland Channel inflow (FSC-inflow), 4: Faroe Bank Channel overflow (FBC-overflow), 5: Denmark Strait overflow (DS-overflow). The illustration is taken from `http://www.oceansites.org/tma/gsr.html`.

The data used is monthly means of the volume transport of the currents in Sv. These were simply plotted against the NAO index as defined by NOAA[2], and a linear fit was found.

On top of this, some radar data of the east-west current in Skagerrak was used in order to see if the link to NAO could be observed. The range of the radar can be seen in Figure 3.2.
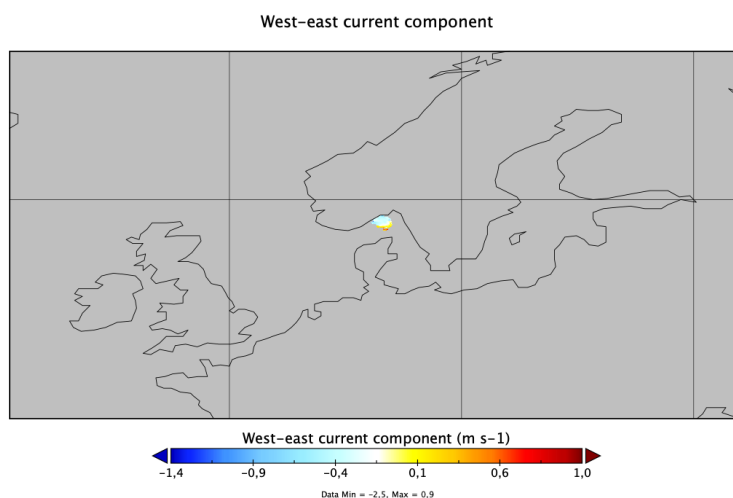
Figure 3.2: A map that shows the extent of the radar measurements of the East-West current in Skagerrak.

This data was taken from a "Copernicus Marine Service" data set called "Global Ocean - in-situ Near real time observations of ocean currents" [3]. The data set is rather short, only ranging from 2020 to present. Therefore daily means of the whole radar area were used in order to get more data points [4]. This is not ideal, since it is doubtful that the response to NAO can happen on these timescales. This data was also regressed against NAO index and a linear fit was performed.

3.2 Empirical Orthogonal Function Analysis

Empirical Orthogonal Function (EOF) analysis is widely used in climate science. It is a method by which it is possible to determine the main patterns of variability of a data set. In this thesis, it is used to analyse the variability of MSLP, OHC, SST, SSH and current speed.

EOF analysis is also called Principal Component Analysis (PCA). EOF analysis is typically used on large spatio-temporal data sets, hence why it is commonly used in climate analysis (Martinson, 2018). When analysing a climatic variable, for example temperature, there will usually be some dependence between temperature in two different places. For instance, if it is hot in point A, it is likely also hot in point B, which is close to A, while there might a point C further away where it is usually cold if A is hot, meaning A and C might be anticorrelated (Martinson, 2018). An EOF analysis searches for such patterns in space, which share the same or similar time variability. This is done by a spatial regression which produces a pattern or map showing the co-varying points (Martinson, 2018). EOF analysis is very valuable, since it simplifies a huge data set into a set of patterns that represent the large part of the variability of the whole data set (Martinson, 2018).

In addition to the spatial patterns of variability (the EOFs), EOF analysis also produces a corresponding time series called the Principal Component (PC)

---

[3]Available here:`https://data.marine.copernicus.eu/product/INSITU_GLO_PHY_UV_DISCRETE_NRT_013_048/description?view=-&task=results&product_id=-&option=-`

[4]The daily NAO index data is available here: `https://ftp.cpc.ncep.noaa.gov/cwlinks/norm.daily.aao.index.b790101.current.ascii`

time series. There is one PC time series per EOF, and it describes how much the given pattern contributes to the variability of the data at each time step.

Climate data can be illustrated in the form of a spatio temporal matrix, F, as illustrated in Figure 3.3, where each row is a map at time t, and each column is the time series for location x (Bjornsson and Venegas, 1997). When doing an EOF analysis, firstly, a co-variance matrix of F is made by calculating $R = F^t F$, assuming F is normalized.

$$F = \begin{bmatrix} x_{11} & x_{12} & \cdot & \cdot & \cdot & x_{1p} \\ x_{21} & + & & & & \\ \cdot & & & & & \cdot \\ \cdot & & & & & \cdot \\ \cdot & & & & & \cdot \\ x_{n1} & & \cdot & \cdot & \cdot & x_{np} \end{bmatrix}$$

A map for time t_1

A time series for location x_1
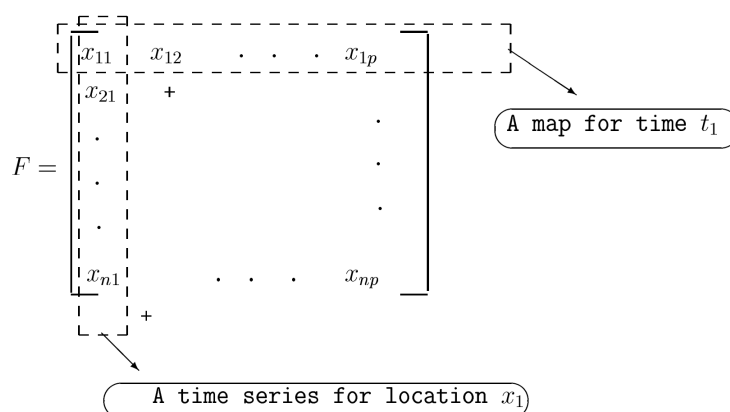
Figure 3.3: An illustration of the spatio-temporal data matrix used for EOF analysis. Each row is a map at time t, and each row is the time series for location x. The figure is taken from Bjornsson and Venegas, 1997.

The co-variance matrix, R, is then used to solve an eigenvalue problem:

$$RC = C\Lambda \tag{3.1}$$

where Λ is a a diagonal matrix of the eigenvalues λ_i of R, and C is a matrix containing the eigenvectors c_i that correspond to the eigenvalues λ_i (Bjornsson and Venegas, 1997).

When solving this problem and finding the eigenvectors and values, the eigenvectors c_i correspond to the EOF patterns, and the eigenvalues λ_i represent how much of the variance in the data each of the patterns represent. The definition of the eigenvector matrix C is such that $C^t C = CC^t = I$, where I is the identity matrix, meaning that the eigenvectors are orthogonal in space.

R can be expressed in terms of eigenvectors and values like so

$$R = \lambda_1 c_1 c_1^t + \lambda_2 c_2 c_2^t + ... + \lambda_p c_p c_p^t \qquad (3.2)$$

where the leading mode of variability, also known as EOF1, is the one that corresponds to the highest eigenvalue, meaning λ_1. Most of the variance of the data can often be described by the first few eigenvalues.

In order to get the time evolution of the EOF1 pattern, also known as the PC time series, the following problem needs to be solved:

$$\vec{a_1} = F \vec{c_1} \qquad (3.3)$$

where $\vec{a_1}$ is an n dimensional vector of the projections of the map in F onto EOF1. $\vec{a_1}$ is therefore a time series evolution of EOF1. This calculation can be done for every EOF, in order to get the different PC time series. In the same way that the EOF are orthogonal in space, the PC time series are orthogonal in time.

These two orthogonality constraints in space and time are the largest caveats of EOF analysis. This means that the analysis assumes that the different modes of variability are completely independent of each other, which might not be the case in the physical world. This will be discussed further in section 5.3

3.3 EOF Analysis in the North Atlantic Sector

The EOF analysis described in the previous section was performed on all the variables that were downloaded from the Copernicus data store. These were MSLP, OHC, SST, SSH, salinity and current speed. This was done in order to be able to identify the main modes of variability for the different variables, as well as being able to compare the PC time series of the modes of variability to identify whether there was some co-variation. All of the variables were analysed at different time resolutions, which were; monthly means, extended winter means, and 5-year running means. It was later decided not to include

the 5-year running means in this thesis. The observed EOF analysis of the 5-year running means can be seen in the Appendix. Since this thesis was exploratory, some of the variables were deemed to not be of great interest for this analysis. These can be found in the Appendix.
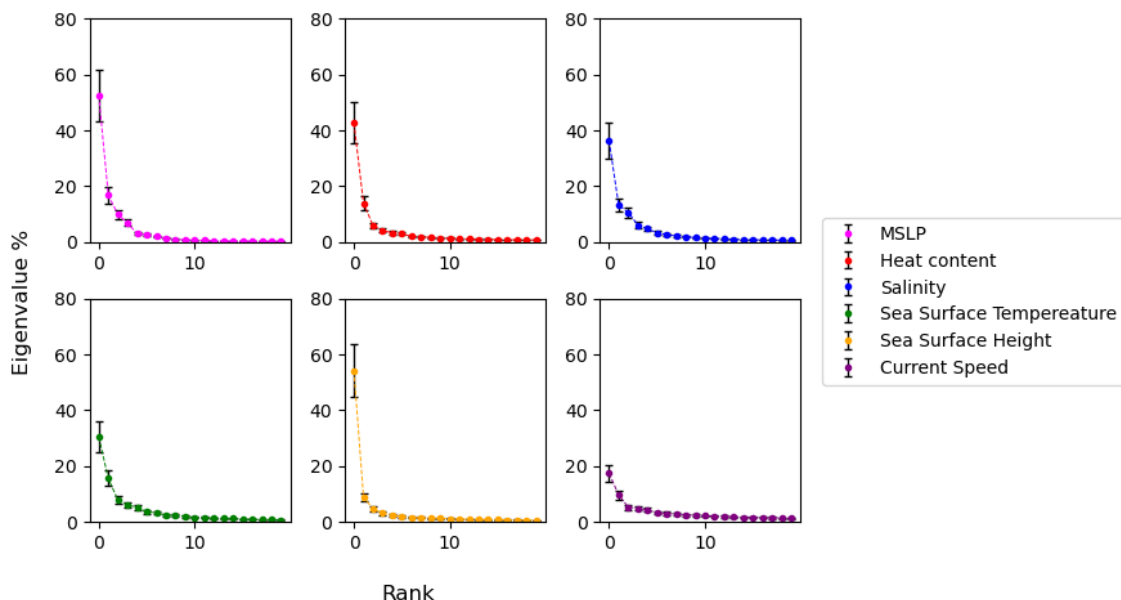
Figure 3.4: Eigenvalue spectrum for each of the variables considered using extended winter means. The explained variance of the 20 first leading EOFs including associated errors.

When doing an EOF analysis, the explained variance decreases with the rank of EOF. This means that EOF1 has the highest explained variance, also the associated error, that is computed according to North's Rule of Thumb (North *et al.*, 1982). Figure 3.4 shows the 20 leading EOFs of all the variables considered in this thesis, along with the corresponding error bars. It can be seen that for most of the variables, the explained variance of the first and the second EOF do not cross error bars. This indicates that the first and second modes of variability are distinct patterns and do not overlap. It can be seen that the second and third EOFs of salinity do indeed overlap. This means that those patterns are not completely distinguishable. Therefore the EOF results for salinity will not be analysed further - they can be found in the Appendix. The EOF analysis of current speed showed a very low explained variance, and therefore they will only be presented in the Appendix. The eigenvalue spectrums shown on Figure 3.4 are based on the extended winter means, because they showed the largest errors, and therefore the largest chance of overlapping. It should be mentioned that EOF2 and EOF3 of salinity also intercept each other when

using monthly means. The eigenvalue spectrums for monthly means can be found in the Appendix.

EOF analysis was also applied to detrended SST and OHC. The eigenvalue spectrums for the detrended extended winter means can be seen on Figure 3.5.
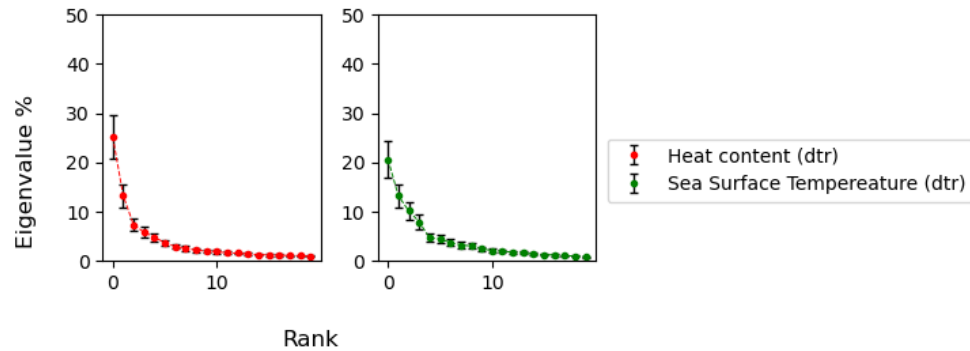
Figure 3.5: Eigenvalue spectrum for the detrended variables SST and OHC using extended winter means. The explained variance of the 20 first leading EOFs including associated errors.

It is clear the EOFs of SST largely overlap after EOF1. This means that the pattern observed in EOF2 can not be distinguished from the others, and can therefore not give meaningful results.

3.3.1 MSLP

The observed EOF patterns of MSLP in the NA region can be seen in Figure 3.6. The different time resolutions are shown. The first two modes of variability for MSLP combined explain ~50% to ~69% of the variability depending on what time average was used.

The first mode of variability, EOF1, shows a pattern of two centers of action, one over Iceland and one of opposite sign over the Azores. This is identified as the NAO and it explains 34% of the variability at monthly time scales.

EOF2 shows a strong center of action south of Iceland, with a ring of opposite sign that surrounds the main center of action. This explains ~17% of the variability. This pattern is recognised as the Atlantic ridge pattern.

(a) Monthly EOF patterns of MSLP

(b) monthly PC time series

(c) Extended winter EOF patterns of MSLP

(d) Extended winter PC time series
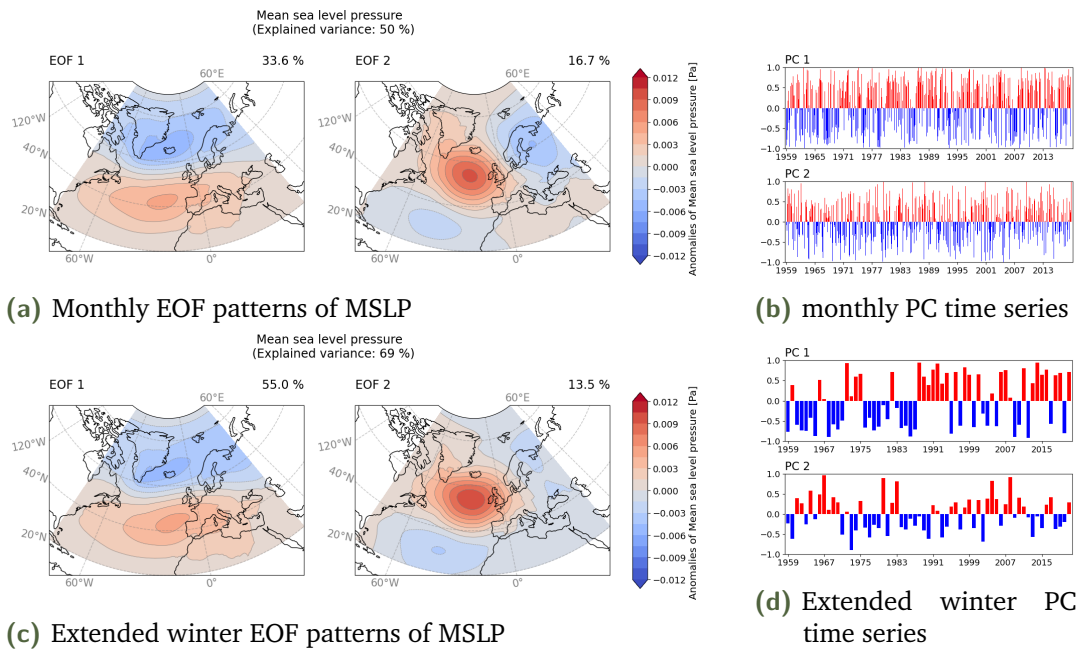
Figure 3.6: The result of the EOF analysis of MSLP. (a), (c): the patterns of the two leading modes of variability for MSLP based on monthly and extended winter(NDJFM) means respectively. (b), (d): the corresponding PC time series of the two leading modes of variability on based on monthly and extended winter means respectively.

Figure 3.6 also shows the PC time series of the EOFs. Looking specifically at PC1, it can be seen that there are phases of the NAO where the PC loading switches sign semi periodically. This becomes clearer when looking at extended winter means in Figure 3.6 (d).

3.3.2 Sea Surface Temperature

The observed EOF patterns of SST can be seen on Figure 3.7. The two first modes explain 34% to 46% of the variance in the SST of the NA ocean, depending on the time scale used.

EOF1 shows an almost uniform pattern that is strongest over the Gulf stream. This pattern was believed to be an AMO signal. There is however a weak center of action south of Greenland, which becomes stronger in the extended winter mean. This pattern explains ~23 % of the variance on monthly time scales. It can be seen in Figure 3.7 (b) and (d) that EOF1 switches sign quite dramatically around 1997, which is in accordance with the switch in AMO index in Figure 2.6. EOF2 shows a stronger tripole pattern (SST-tripole) with

(a) Monthly EOF patterns of SST

(b) monthly PC time series

(c) Extended winter EOF patterns of SST

(d) Extended winter PC time series
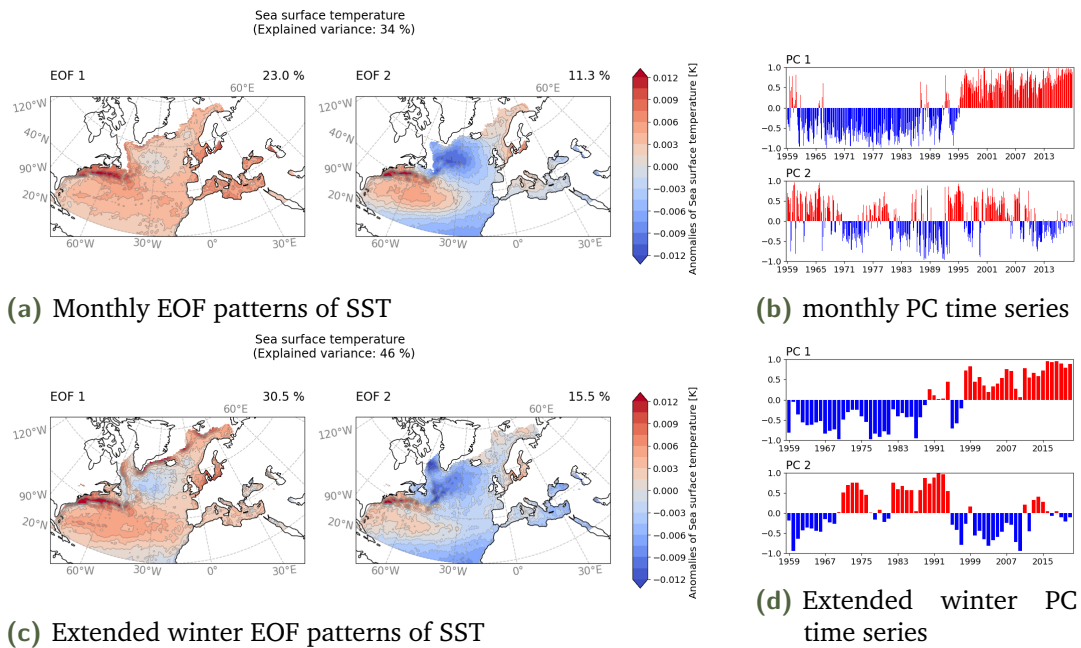
Figure 3.7: The result of the EOF analysis of SST. (a), (c): the patterns of the two leading modes of variability for SST based on monthly and extended winter(DJFMA) means respectively. (b), (d): the corresponding PC time series of the two leading modes of variability on based on monthly and extended winter means respectively.

one strong center of action over the Gulf stream and one south of Greenland, while the edge of a third center of action can be seen off the coast of Africa. This is the pattern that explains most of the residual variation, which includes the influence from the NAO. The extended winter mean is shifted one month compared to the MSLP extended winter mean. This is due to time lag, which will be explained in detail in the Results section.

An EOF analysis was also performed on detrended SST. As seen in Figure 3.5, there was an overlap of the second mode of variability with the third (and higher) mode of variability. Therefore, only EOF1 of the detrended SST can be used further in the analysis. The EOF analysis results for SST can be found in the Appendix in Figure 8.5, and it can be seen that detrending removed the AMO signal. The reason for this will be discussed in the Discussion.

3.3.3 Ocean Heat Content

The results of the EOF analysis of OHC can be seen on Figure 3.8. The first two leading modes of variability of OHC explain 43% to 56% of the variability.

(a) Monthly EOF patterns of OHC

(b) monthly PC time series

(c) Extended winter EOF patterns of OHC

(d) Extended winter PC time series
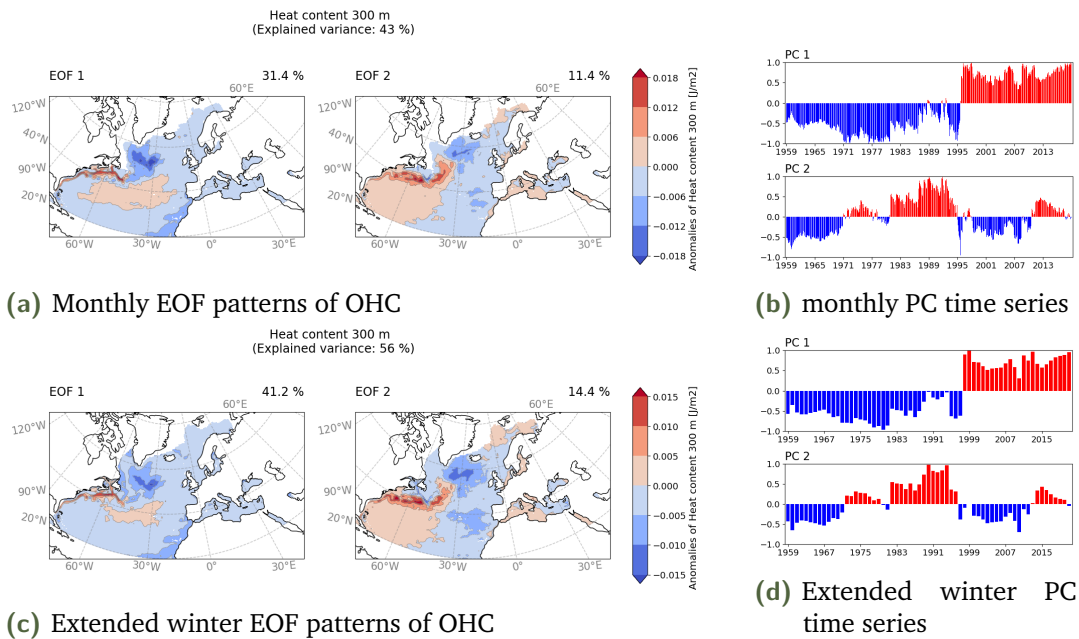
Figure 3.8: The result of the EOF analysis of OHC. (a), (c): the patterns of the two leading modes of variability for OHC based on monthly and extended winter(DJFMA) means respectively. (b), (d): the corresponding PC time series of the two leading modes of variability on based on monthly and extended winter means respectively.

The patterns of EOF1 and EOF2 do resemble each other with an action center where the Gulf stream is and one of opposite sign south of Greenland, and this does correspond to the findings from the EOF analysis of SST. However, the pattern in EOF1 is much more concentrated spatially with a very narrow Gulf stream.

EOF1 explains 31% to 43% of the variance depending on the time average, and from the PC time series it was thought to be the same signal that was seen in EOF1 of SST, the AMO, with a dramatic phase shift around 1997. EOF2 explains 11% to 14% of the variance and is thought to be the variations that come from atmospheric interactions such as NAO, as for EOF2 of SST. The EOF analysis results for detrended OHC can be found in the Appendix. It can be seen that the modes are the same after detrending.

3.3.4 Sea Surface Height

The first two leading modes of variability of SSH can be seen in Figure 3.9. They explain 47% to 63% of the variance. Both EOF1 and EOF2 have height

(a) Monthly EOF patterns of Sea Surface Height

(b) monthly PC time series

(c) Extended winter EOF patterns of Sea Surface Height

(d) Extended winter PC time series
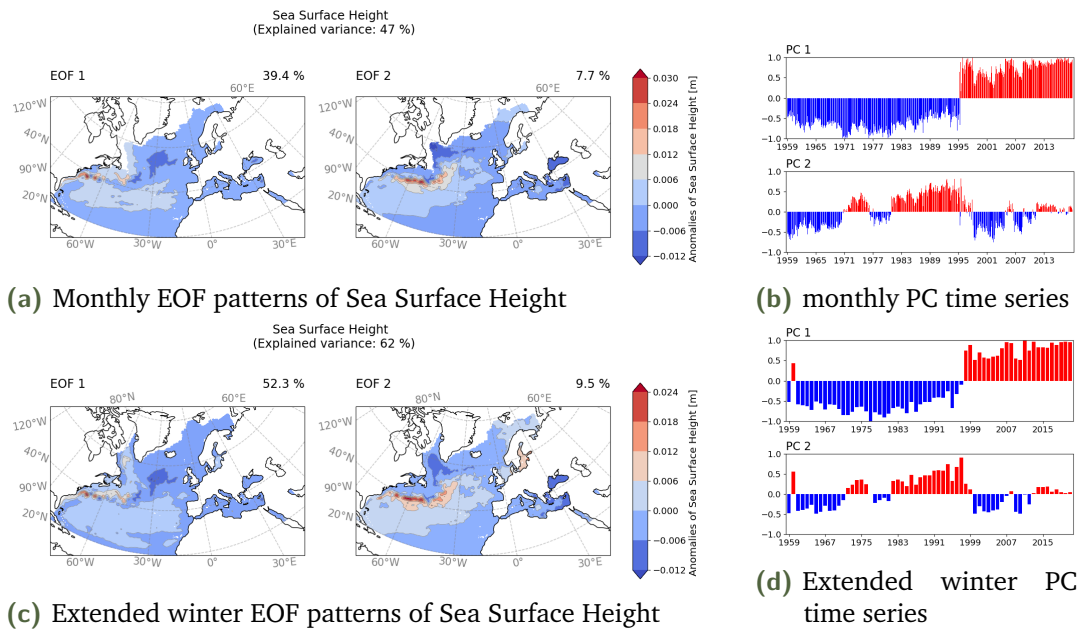
Figure 3.9: The result of the EOF analysis of Sea Surface Height. (a), (c): the patterns of the two leading modes of variability for Sea Surface Height based on monthly and extended winter means respectively. (b), (d): the corresponding PC time series of the two leading modes of variability on based on monthly and extended winter means respectively.

anomaly patterns along the Gulf stream, which are a result of the meandering of the Gulf stream. EOF1 has more concentrated areas of anomalies, while the pattern in EOF2 covers a larger area. Like for the other variables, EOF1 was believed to be the AMO variability, which can be identified from its PC time series. It explains 39% to 54% of the variance. EOF2 explains 8% to 10% of the variability, which is very low. It is however, closely linked to MSLP. This will be analysed more in detail in Section 4.1.

3.4 Time Lag

In order to determine if there was any lag between NAO forcing and the respective variables, the PC time series were compared. If they co-vary, this can be an indicator of the NAO affecting the oceanic variables.

In order to explore whether the NAO leads or lags ocean circulation changes, a cross correlation analysis was made. This was done by taking the data in monthly means, and then shifting the one time series by one month at the

time, and doing a Pearson correlation analysis each time one data set was shifted by a month. Pearson correlation coefficient is defined as

$$r = \frac{cov(X, Y)}{\sigma_x \sigma_y} \tag{3.4}$$

where the co-variance of variable X and Y is divided the product of the standard deviations of variable X and Y.

This leads to a correlation value for each month of the data set. The amounts of shifts that have been done when the highest correlation is found determines the lag between the time series.

3.5 Principal Component Regression Analysis

The results from the EOF analysis were also used to perform a PC regression analysis. In order to do this, the time series of the anomalies in a grid point is compared to the PC time series of the different modes of variability. This thesis explores the linkage between NAO and various oceanic variables. Therefore the variables are compared to the the first mode of variability for MSLP, which is identified to be NAO as mentioned above.

If the time series in a grid point co-varies with the PC time series, it can be concluded that the grid point may be causally related to the NAO. The analysis calculates a linear regression coefficient for each grid point using ordinary least-square fit regression. The regression coefficient indicates how strong the relationship is between the PC time series and the grid point and whether the relationship is positive or negative.

In order to see which points were highly correlated to the NAO, a correlation maps was also made by correlating the time series in each point to the PC loading of the NAO. Then, in order to determine which points were significantly correlated to the NAO, all points with a Pearson correlation coefficient below 0.3 were filtered out of the PC regression map.

Results

This section presents what effect the NAO has on the oceanic variables through comparison of the PC time series. A lag between NAO and the oceanic variables will be determined using cross correlation. A PC regression analysis will also be presented, where the oceanic variables have been regressed onto MSLP. And lastly, a simple linear regression is performed between the NAO index and observational data of ocean currents, to determine if there is a NAO signal in direct measurements of ocean currents.

4.1   Comparison of PC Time Series

In order to identify whether some of the patterns co-varied in time, the PC time series of interests were compared. A cross correlation was made of PC time series for each variable compared to the first EOF of MSLP, which will now be referred to as NAO.

To better understand which of the cross correlations can actually be interpreted as a robust signal, the correlation was plotted against the lags. This can be seen in Figure 4.1. The graphs indicated in green have a clear signal and comparatively little noise, while the graphs indicated in red either have no signal or too much noise to deduce a clear result.

The result of these cross correlations can be seen in Table 4.1. The variables marked in green are the same variables that are marked in green in Figure 4.1. Normally, p-values as low as those in Table 4.1 would be considered statistically significant, most of them extremely so. They have, however, been calculated without taking into account auto-correlation, which may reduce the degrees of freedom drastically. Varying the lag to optimize the correlation will also reduce the degrees of freedom. This will be discussed further in section 5.3.
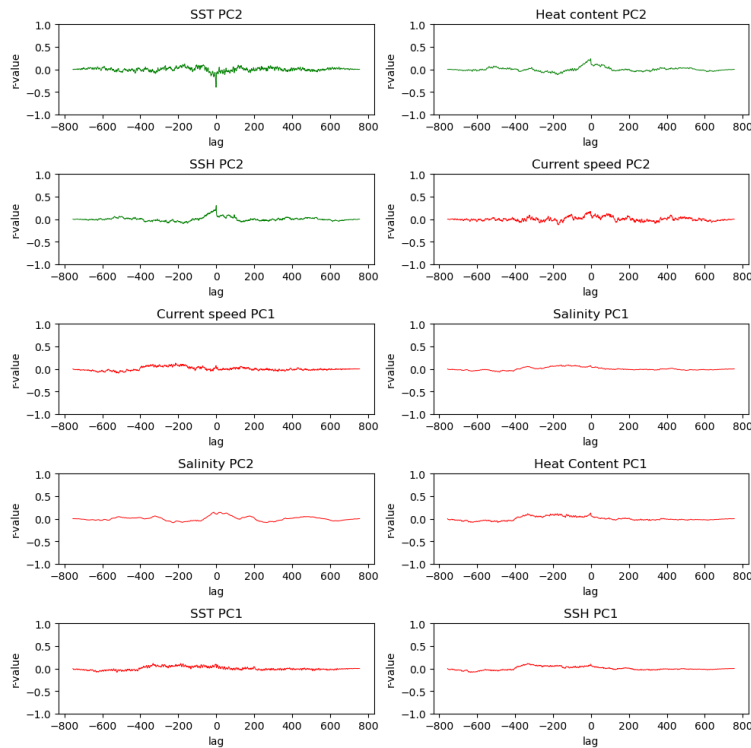
Figure 4.1: The cross correlated lags between the respective variables and MSLP.

Table 4.1: The Pearson correlation coefficient, r-value, and the associated p-value and time lag in months between the first PC time series of MSLP (NAO) and the different variables indicated in the table. A negative lag means that MSLP is leading.

	r-value	p-value	lag
SST PC1	0.1127	0.00191	-187
SST PC2	-0.3988	3.104 e-30	-1
OHC PC1	0.1281	0.0004	-1
OHC PC2	0.2345	6.6012 e-11	-1
SSH EOF1	0.1128	0.0019	-333
SSH EOF2	0.3022	1.977 e-7	0
Current EOF1	0.1299	0.0003	-214
Current EOF2	0.1723	1.8907 e-6	-3
Salinity EOF1	0.0889	0.0144	-120
Salinity EOF2	0.1433	7.599 e-5	-13

These cross correlations were also done for detrended SST and OHC, and the results can be seen Table 4.2, while the correlations plotted against lags can be seen in the Appendix in Figure 8.7. The reasoning behind deeming SST PC1 and OHC PC2 to be marked in green is based on the fact that these are the well known SST tripole, which is related to the NAO, as mentioned in the

Table 4.2: This table shows the same as Table 4.1, but with detrended SST and OHC

	r-value	lag
SST PC1	-0.38	-1
SST PC2	0.13	-67
OHC PC1	0.20	-1
OHC PC2	0.19	-13

Background. This can be seen in the EOF patterns and the PC time series in the Appendix in Figures 8.5 and 8.6.

Based on the numbers in Table 4.2, PC1 of OHC looks like it could be related to the NAO. But looking at PC1 of detrended OHC in Figure 8.6, it can be seen that this resembles the AMO signal more, since it does not fluctuate like the NAO signal at all.

Using the results from Figure 4.1 and Table 4.1 and 4.2, the PC time series that show a sufficient correlation with NAO were analysed in greater depth. In this analysis, both the detrended and non-detrended PC time of OHC series will be considered.
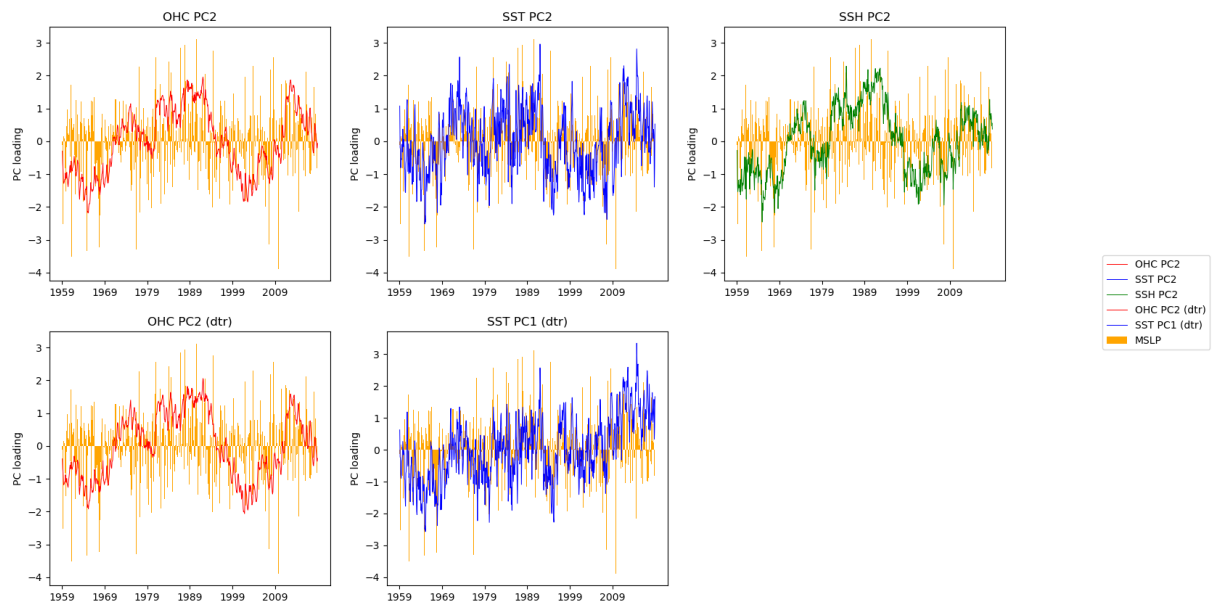
Figure 4.2: The comparison of the standardized PC time series for NAO and the oceanic variables that were deemed of interest.

Figure 4.2 shows the comparison of NAO with the PC time series before mentioned. It can be seen that the data is very noisy, especially the PCs for

SST. There is, however, some degree of visible correlation in the "OCH PC2" and "SSH PC2" plots, but in general, they are too noisy to deduce much from. Because of this, efforts to reduce the noise have been made using an analysis of the data points where the NAO PC time series was $>\pm1$ std (the data was standerdized). This will be shown in the following section.

4.1.1 NAO Loading of more than ±1 std

The results from the analysis where the NAO PC loading was $>\pm1$ std can be seen in Table 4.3. The r value was found from a Pearson correlation. The lag was found by first shifting one data set by x months relatively to the other, and then filtering the data, so that only data points where NAO PC loading was $>\pm1$ std were included. The process of shifting by one month at a time was repeated until the highest correlation was found, which then determined the lag in months.

It can be seen that the correlations are higher in Table 4.3 than the corresponding values in Table 4.1. This is in line with what is expected, since a more extreme NAO pattern, positive or negative, should influence the other variables more.

Table 4.3: The Pearson correlation coefficient and lag in months of the oceanic variables compared with NAO where the PC loading of the NAO was $>\pm1$ std. Negative lag means NAO is leading.

	r-value	lag
SST PC2	-0.61	-1
OHC PC2	0.44	-2
SSH PC2	0.52	0
SST PC1 (dtr)	-0.57	-1
OHC PC2 (dtr)	0.39	-1

The comparison of the PC time series based on the findings in Table 4.3 can be seen in Figure 4.3. It can be seen that in general the variables do co-vary much more in the analysis in Figure 4.3 than in Figure 4.2.
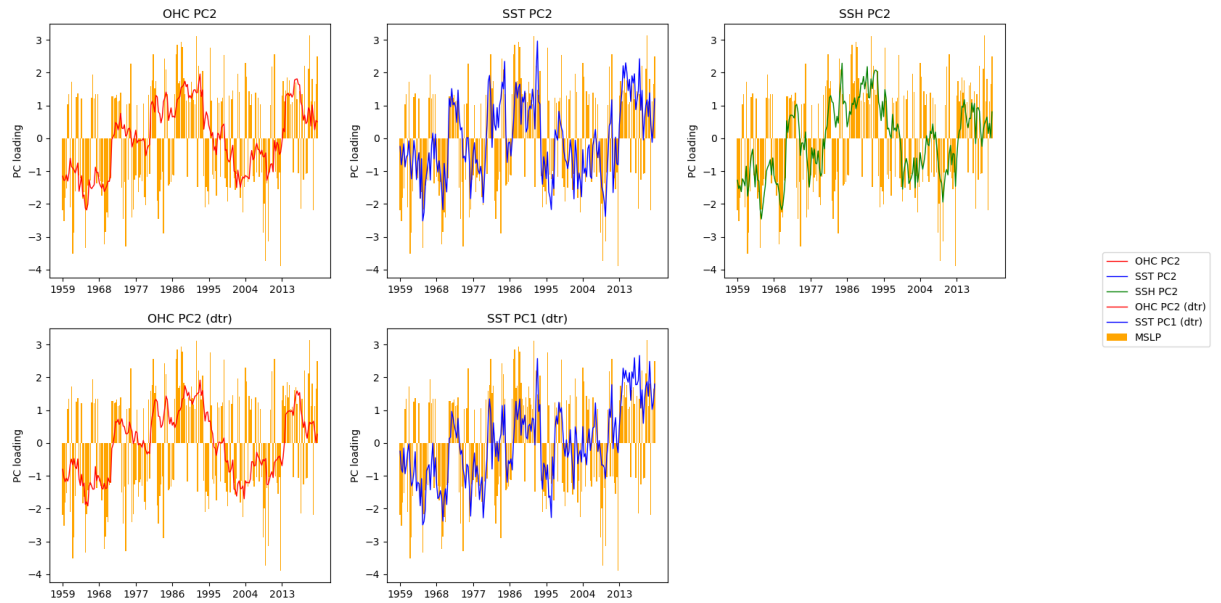
Figure 4.3: The comparison of the standardized PC time series for NAO and the oceanic variables that were deemed of interest, using the values where the NAO PC loading was $> \pm 1$ std.

4.1.2 Extended Winter PC time Series

Another way to tease out results from noisy data is to use longer time averages. The PC time series from the extended winter means will now be analysed in the same fashion as the monthly data was earlier. The lag that were found in Table 4.1 and 4.2 were used. The lags found in the $< \pm 1$ std analysis were slightly different than the lags found in the monthly mean analysis. These lags will not be used, however, since the extended winter data will not be analysed based on if the NAO forcing is $< \pm 1$ std. It should also be mentioned, that for OHC the lag of 1 month was used, even though the lag for detrended OHC was found to be 13 months. The reason for this will be elaborated on in the Discussion. For MSLP the extended winter months Nov-Mar was used, but for SST and OHC the extended winter Dec-Apr was used since the NAO was found to be leading by one month. There was no lag for SSH and therefore the months used for SSH were also Nov-Mar. The results of this analysis can be seen in Figure 4.4, where the r and p- values are displayed on each graph. Gaussian smoothing was performed onto the PC time series in Figure 4.4, the smoothing window being 3 winters. The result of this can be seen in Figure 4.5.
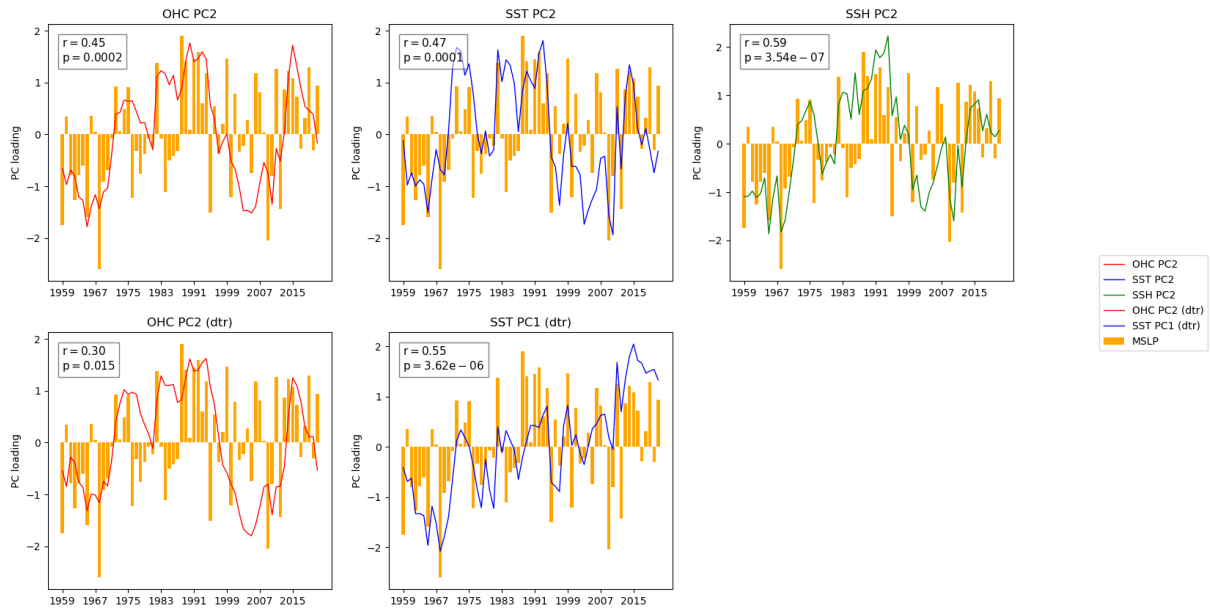
Figure 4.4: The comparison of the standardized PC time series for NAO and the oceanic variables that were deemed of interest, using the PC time series from the extended winter EOF analysis. r- and p-values are expressed on each graph.
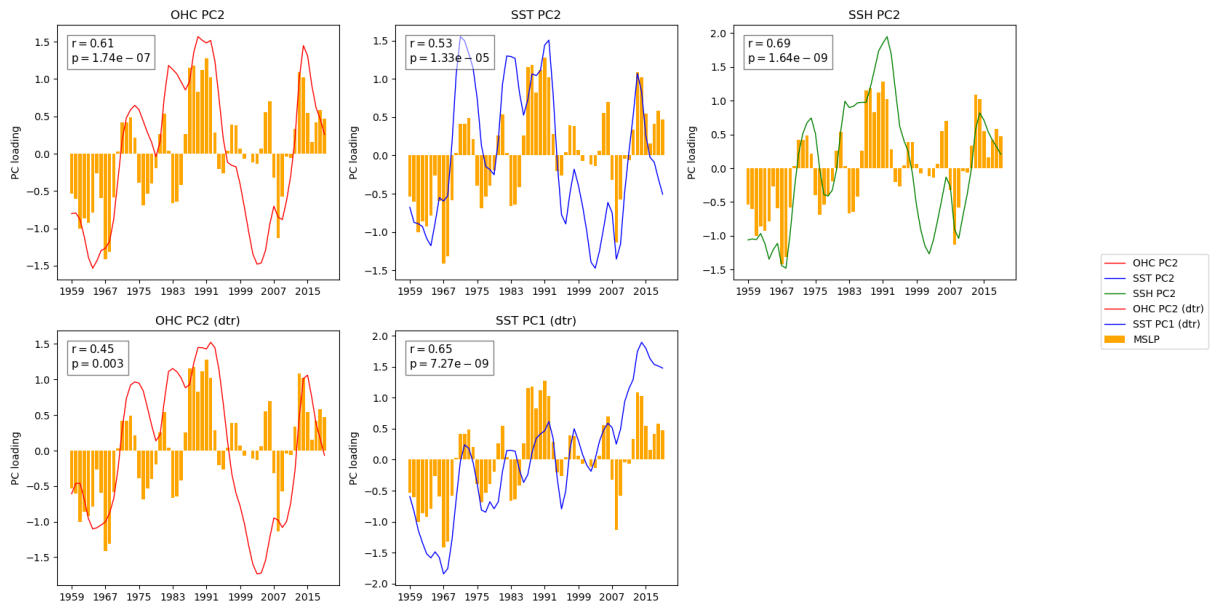
Figure 4.5: The comparison of the standardized PC time series for NAO and the oceanic variables that were deemed of interest, using the PC time series from the extended winter EOF analysis, where Gaussian smoothing was applied to each variable, with a window of 3 years. r- and p-values are expressed on each graph.

Visually, for both of these figures, it can be seen that the NAO leads the OHC slightly in both the detrended and non detrended case. And a cross correlation analysis was performed. Indeed NAO leads OHC by one year with an r-value of 0.46 for 'OHC PC2' and 0.37 for 'OHC PC2 (dtr)'.

4.2 Principal Component Regression Analysis

The Principal Component analysis was made in order to identify what areas were more and less influenced by NAO. The PC regression analysis was done for all variables, where they were individually regressed onto the first mode of variability for MSLP. In this analysis, all the variables will be considered, since this doesn't have anything to do with whether the EOF patterns co vary. It simply asks the question, does this grid point vary with the NAO loading?

The PC regression was based on extended winter means for SST, OHC and SSH using the same lags as described in Section 4.1.2. This was done in order to reduce noise. Since no meaningful lags were found for current speed and salinity in the lag analysis, the season Nov-Mar was used. Current speed was split up into zonal and meridional components for this analysis. Only grid points with correlations higher than 0.3 were plotted in the regression. The results from the PC regression can be seen in Figure 4.6. All of the correlation maps can be seen in the Appendix, as well as the unfiltered PC regression maps.

It can be seen that there are the patterns for SST and OHC are similar (Figure 4.6 (a), (b), (c) and (d)), whit the regression for SST being stronger. It can also be seen that detrending the data in general made the correlation and regression coefficients lower. There is an area of negative correlation south of Greenland, meaning that this area cools with stronger positive NAO. And there is a band of warming with strong NAO in the subtropical NA off the East coast of the US. This is known as the SST tripole which has been mentioned previously.

The PC regression analysis for SSH in 4.6 (e) showed that NAO has a strong positive regression coefficient with the sea level in the Baltic sea and across

(a) PC regression between SST and the leading mode of MSLP

(b) PC regression between detrended SST and the leading mode of MSLP

(c) PC regression between OHC and the leading mode of MSLP

(d) PC regression between detrended OHC and the leading mode of MSLP

(e) PC regression between SSH and the leading mode of MSLP

(f) PC regression between salinity and the leading mode of MSLP

(g) PC regression between Zonal velocity and the leading mode of MSLP

(h) PC regression between Meridional velocity and the leading mode of MSLP

Figure 4.6: PC regression maps between all variables individually and the first mode of MSLP, the NAO.

the Atlantic, and with a slight negative regression coefficient with SSH around Iceland.

The PC regression for salinity in Figure 4.6 (f) basically showed no correlations higher than 0.3. This might be due to the fact that it was averaged over 300 meters depth, and therefor the atmospheric influence was small. It could also be due to the fact that the area which was used in this analysis was very compromised in order to avoid variances in the salinity that were related to other physical processes.

The PC regression analysis of the current velocities in 4.6 (g) and (h) in general show very small regression coefficients, except for in Skagerrak. When looking at the correlation maps in the Appendix, Figure 8.8, it can be seen that the correlations between the zonal current and NAO are really high in the Baltic Sea, the North Sea, and between Iceland, Faroe Islands and Scotland. This might be due to increased wind driven currents caused by the low pressure over Iceland.

The next step was to link the findings of these PC regressions to actual observed data of ocean currents. This will be done in the next section.

4.3 Linking EOF Findings to Observed Data

The NAO index data was taken from NOAA, and the Volume transport across the Greenland-Scotland ridges was accessed through the Faroese Marine Research Institute. Only the extended winter months were used (Nov-Mar).The volume transport plotted against NAO index can be seen in Figure 4.7. This is the data from two locations, the Faroe Current and the Faroe-Shetland Channel inflow. These locations can be seen in Figure 3.1.

It can be seen that there is a tendency that with higher NAO index, the volume transport increases for the FSC, but no NAO dependency can be seen for the IF. Both the correlation and the slope of the regression line is larger for the FSC volume transport than for the IF. The r-squraed values are quite low. This is, however, to be expected, as there are many other factors that come into
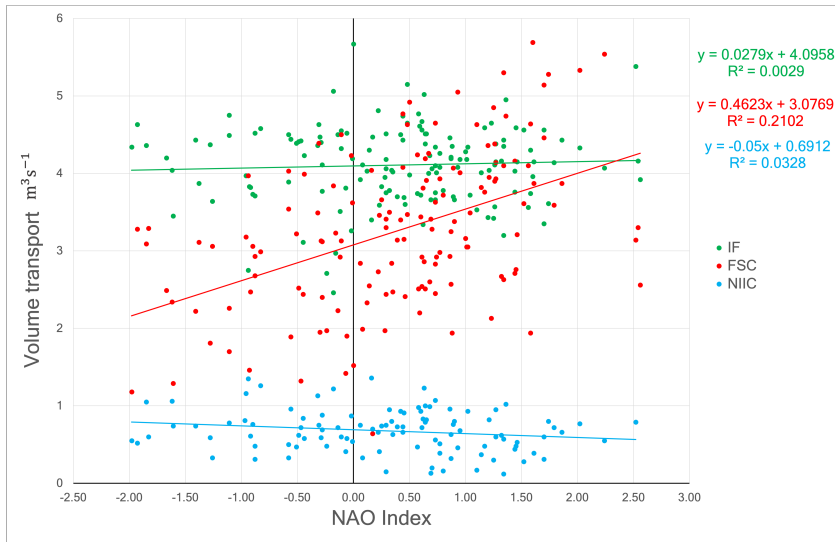
Figure 4.7: Volume transport in the Faroe Current(green) and the Faroe-Shetland Channel (red) plotted agains NAO index as defined by NOAA.

play other than the NAO. Also the volume transport is the total inflow in the respective channels, not just surface currents. Therefore, it is not as affected by the atmosphere.

The observational data in Skagerrak was also plotted against the NAO index. Once again, only the extended winter months were used (Nov-Mar). The result can be seen in Figure 4.8. The r-squared value is much lower here than in Figure 4.7. But the data does not prove that there is no correlation between NAO and current speed, and a small negative trend can be seen.
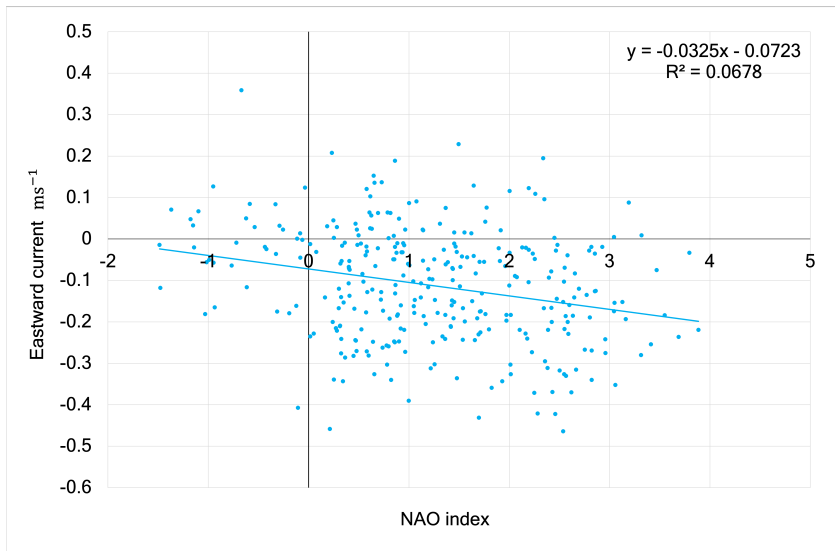
Figure 4.8: Radar measurements of the eastward current speed in Skagerrak plotted against NAO index as defined by NOAA.

Discussion

<div style="text-align: right; font-size: 3em;">5</div>

This chapter discusses the results from the analysis. Firstly, it will dive into how the individual oceanic variables are affected by the NAO and why. The time lag analysis will also be discussed for each variable as well as the PC regression results. Secondly, the observational data analysis will be discussed, as well as the linkage between the observational data and the PC regression results. The limitations and perspectives of this thesis will be discussed.

5.1 NAO and the Oceanic Variables

From the comparison of the PC time series, it was evident that the PCs that co-varied the most with the NAO were the second modes of SST, OHC and SSH. SST and OHC will be discussed together, as they are closely related. SSH will be discussed separately, and the other variables (current speed and salinity) will be discussed together.

5.1.1 SST and OHC

The first modes of SST and OHC looked like an AMO signal due to the dramatic phase shift in the late 1990s, as seen in Figures 3.7 and 3.8 (Enfield *et al.*, 2001). It is, however, hard to conclude that this shift was only attributed to AMO, especially for SST and OHC. The shift might be a mix of the AMO signal and the global warming signal, since the PC loading changes nearly linearly from negative to positive in the time period of interest in this study (1959-2022), which indeed also looks like a global warming signal. It is therefore hard to distinguish between AMO and global warming for this time period.

After detrending SST and OHC, the issue with conflating the AMO signal with a global warming signal became clearer. Detrending SST and OHC made the modes of variability somewhat ambiguous - for SST, the AMO signal was

largely removed, as seen in Figure 8.5. The pattern in EOF1 became the well known SST tripole pattern that is associated with the NAO, and the monopole associated with AMO was no longer visible. However, when looking at the PC1 time series for detrended SST, there is still a somewhat linear trend, meaning that the detrending did not necessarily remove either a global warming signal or the AMO signal. This slight linear trend was amplified in the PC comparison for the smoothed extended winter means in Figure 4.5. This result plays into the disputes around whether AMO is an oscillation caused by changes in the AMOC, or if it is caused by anthropogenic climate change (Trenberth *et al.*, 2019).

Detrending OHC did not display a similar result. In this case, the first mode of variability could still be argued to be AMO. This could be due to the fact that the global trend of OHC which was removed from each point was not exclusively a warming trend. There was an initial period of cooling in the 1950-1980s, which could have been what made the difference in detrending SST compared to detreding OHC, since in the global trend for SST there was only heating. This is to be expected, since the global warming signal is expected to be visible in OHC later than for SST due to a lag as heat propagates into the deeper ocean.

This resulted in the NAO signal being compared to the second mode of variability of SST and OHC, when not detredned, and SST to the first mode of variability, when detrended, as the first mode of variability is the SST tripole post-detrending.

The second modes of variability of SST and OHC (first mode for detrended SST) were found to co-vary with NAO. The co-variance became especially clear in the ± 1 std analysis and extended winter mean analysis in Figures 4.3, 4.4, and 4.5. The monthly mean comparisons in Figure 4.2 were too noisy for a conclusion to be made. On average, the highest correlations with r-values of around 0.3-0.6, between SST, OHC, and NAO were found in the filtered monthly PC comparison where the NAO loading was $> \pm 1$ std. This is to be expected, since a stronger NAO forcing should give stronger responses in the ocean(Hurrell and Visbeck, 2003). The extended winter means also gave reasonably high correlations between OHC, SST, and NAO with r-values of around 0.3-0.65. This means that the NAO loading was moderately to highly correlated to SST and OCH, with some variations depending on variation

based on if detrending was performed or not and which time average was used.

This is in accordance with other findings, where the SST tripole pattern (EOF2 of SST and OHC) is commonly known to be induced by NAO, which has been proven many times in literature (Hurrell and Visbeck, 2003). The r-values of OHC response to NAO were weaker than for SST, which is not surprising since the OHC was in 0-300m depth. This will naturally not be influenced as much and as promptly by the atmosphere as SST. The reason for this tripole pattern that can be seen in Figure 3.7 is a change in circulation and therefore a change in heat distribution. This is also the reason for the pattern for OHC, which can be seen in Figure 3.8.

The cross correlation analysis was done on monthly scales and showed that the NAO loading leads the SST and OHC loading by one month. This confirms the fact that in general the ocean lags the atmosphere on timescales shorter than a decade, and other studies have found the lag to be of the same magnitude (Hurrell and Visbeck, 2003) (Pan, 2005). The discrepancy in the cross correlation results for OHC depending on whether it is detrended or not as seen in Tables 4.1 and 4.2 could be attributed to the fact that in the cross correlation, OHC has a "tail" of high correlations. This means that the response to NAO in the upper ocean is longer than on the surface due to circulation delaying the signal. After detrending, the "tail" became more of a plateau, which is the reason why the OHC was found to lag the NAO by 13 months when detrended. This can be seen when comparing Figures 4.1 and 8.7. When looking at the PC comparisons between OHC and NAO on Figure 4.5, NAO leads OHC by a year, which can also be attributed to this 'tail' that can be seen in the cross correlation, and again confirms that the response time in the upper ocean is much longer than on the surface.

It should be mentioned that other studies find that there is a positive feedback loop between the SST tripole and the NAO (Pan, 2005). However, in Figure 4.1 it can be seen that there are quite dramatic drop offs in the correlations after the maximum correlation has been reached. This indicates that the SST tripole does not simultaneously lead and lag the atmosphere (positive feedback). The reason for this is that the time scales are too large to be able to discern this. In Pan, 2005, they find that the intrinsic time scale of the NAO is around 10 days,

meaning that a much finer time resolution is needed to observe the positive feedback loop.

When looking at the PC regressions on Figure 4.6, it was clear that there was indeed a tripole pattern when the variables were regressed onto the NAO signal. The tripole was not as clear for OHC as for SST. This was expected because, as mentioned before, the OHC is not as well correlated with changes in the atmosphere as SST is on these timescales. The regression coefficients and correlations became smaller after the variables were detrended, especially for the warm center of action. This is also to be expected, since global warming does contribute to this signal in the warming region, and possibility also in the cooling region south of Greenland (Masson-Delmotte *et al.*, 2021). The temperature varied ± 1 degrees Kelvin with the NAO loading, or in the case of OHC it was $\pm 8 * 10^8$ Jm^{-2}.

5.1.2 SSH

SSH was the variable that co-varied the most with NAO, as can be seen in Figures 4.2, 4.3, 4.4, and 4.5. The Pearson correlation coefficient was 0.3 in the monthly mean analysis and went up to 0.7 for the three winter smoothed means, that were done for noise reduction. There was no lag found between SSH and NAO. Sea level height anomalies are normally quick to respond to forcings, especially on continental shelves, due to the effect of sloping topography (Hughes and Meredith, 2006). However, there are studies that show some lag between forcings and SSH anomalies on the open ocean (Hughes and Meredith, 2006). This lag was not observed in this analysis, but it might have become apparent if the areas were separated into smaller sections, for example the Baltic and the open ocean, since the response times in SSH anomaly are expected to be different in the open ocean compared to a continental shelf.

In the PC regression analysis of SSH onto NAO on Figure 4.6 (e), it can be seen that there are strong positive trends between NAO loading and SSH in the Baltic Sea and the southern NA, while there are a weaker negative trends in the northern NA and the Mediterranean, this is as found in Iglesias *et al.*, 2017. In particular the SSH in the Baltic is strongly correlated with the NAO, as can be seen in the Appendix in Figure 8.8. The change in SSH with NAO

loading is ± 0.1 m, which is of the same order of magnitude as was found in Esselborn and Eden, 2001, where the response of a single switch in NAO forcing was studied in the subpolar gyre.

5.1.3 Salinity and Current Speeds

It can be seen throughout the methods and results both salinity and current speed were not considered in EOF and PC comparison analysis and the time lag analysis.

In the case for salinity, the area of interest was compromised quite dramatically due to the fact that a lot of the area had to be masked out in order to get rid of the variations from sea ice, run off, and the dramatically different values of salinity in the Baltic Sea and the Mediterranean. This caused the pattern observed in the EOF analysis of salinity to be compromised, as can be seen in the Appendix Figure 8.3. Because of this, no conclusions could be drawn on whether EOF2 of salinity varies with NAO. Other studies have shown that salinity is influenced by the NAO. In Sarafanov, 2009 it was found that the a persistent negative (positive) NAO results in increase (decrease) in temperature and salinity in the intermediate–deep water column in the subpolar gyre. The PC regression of salinity and NAO also did not give any results. This was because the correlations were lower than 0.3 in almost all grid points. The results of the PC regression might have been better if a meaningful lag was found in the first part of the analysis, but this would require a better representation of the EOFs of salinity in the first place. Another reason for inconclusive results for salinity could be that a 0-300m weighted average was used instead of just the top layer. This might be too deep to be able to conclude if there was any effect from the NAO.

The current speed EOF analysis can also be found in the Appendix in Figure 8.4. The reason it was only included in the Appendix was because the explained variance of the two first modes of variability were quite low compared to the others, as can be seen in Figure 3.4. This meant that they were considered too noisy to analyse further and to get any meaningful lag analysis out of. For the latter part of the analysis, the currents speed was split up into zonal and meridional components, and only the top layer was used. This was done to see more detail in the correlation maps and the PC regression. The reason for

using the weighted average of the currents on 0-300m depth in the first half of the analysis was, as mentioned in the Background, that one would expect to see an effect from the Ekman transport to be at 300m depth, unfortunately this was not the case (Hurrell and Visbeck, 2003).

The correlation maps between NAO and the current speed, can be seen in the Appendix in Figure 8.8 (g) and (h). It shows that especially the zonal current (positive eastward) is highly correlated to the NAO around Scandinavia and across the GSR. This is as expected, since the intensified westerlies move water masses towards Scandinavia. The meridional current (positive northward) does not show as much correlation to the NAO loading.

When doing the PC regression analysis it was clear that even if the area around Scandinavia and between Scotland and Iceland has a high correlation, the linear regression coefficient was low in most places. This can be seen in Figure 4.6. The current speed varied by ± 0.1 m/s with NAO loading. Especially in Skagerrak, there is a high correlation and high linear regression coefficient. The reason for this strong influence from the NAO on the eastward current in Skagerrak could be the SSH anomalies in the Balitc sea that arose from the NAO, resulting in a stronger current in and out of the Baltic Sea. Also, the current is pushed into a narrow strait.

In summary, the results from the PC time series comparisons and the PC regressions have proved that the SST tripole pattern is closely linked to the NAO and lags the NAO by one month on shorter timescales. This link can also be seen in the OHC with the same time lag. The NAO and SSH were also shown to be closely linked with no time lag. Especially in the North and Baltic Sea, the SSH was strongly positively correlated with the NAO. The zonal current speed was found to be strongly correlated to the NAO around Scandinavia and across the GSR. However, the regression coefficients was not that strong in most places.

5.2 Linking Findings to Observational Data

The correlations in the locations where the observational data was from were very high. The locations can be seen on Figure 3.1 and 3.2. But the linear regression coefficients were quite low in most places. This is to be expected, since this is quite noisy data, as established when doing the EOF analysis of the current speed.

As mentioned before, the observational data across the GSR was measured in volume transport across the ridge but split up into the individual currents. The result from plotting the volume transport against NAO index can be seen in 4.7. It is clear that NAO has some effect on the volume transport for the FSC current, but no effect for the NIIC and IF current. This could be because the FSC current is in line with the intensified storm track that is induced by the NAO and points north-east. Whereas the IF and NIIC currents both bend around the Faroes and Iceland respectively, and are measured directly north of the islands, where the currents flow directly eastward, and hence not in directly in line with the storm track. Since there is no net meridional flow, it also means that when more water is flowing into the Norwegian Sea, the outflow must also be higher. Most of the outflow from the Norwegian Sea occurs in the western region, between Greenland and Iceland and between Iceland and the Faroe Islands, while most of the inflow happens between the Faroe Islands and Shetland. This means that it is expected that the FSC current should be the one that is most highly affected by the NAO. The r-squared value of the regression line between FSC and NAO is 0.21, which is quite low, but simultaneously surprisingly good when considering that this is the volume transport for the whole FSC current. The regression coefficient is 0.41 m^{3}s^{-1} per "NAO index".

As mentioned in the previous section, the ideal place to look for a relationship between NAO and current speed would be in Skagerrak. Unfortunately, there are no regular measurements of currents in this area. The most readily available data that could be found within the scope of this thesis was the radar data in Skagerrak. The mean eastward current measurements that were plotted against NAO index in Figure 4.8 showed a hint of a correlation,

but the r-squared value was very low. The tendency was negative, meaning that with a positive NAO, the current speed westward intensifies. This is in accordance with the PC regression analysis in Figure 4.6 (g), because, upon close inspection, a small counter current positioned up against the Norwegian coastline can be seen (especially in the unfiltered PC regression map in Figure 8.9 (g). It therefore makes sense that the average current the radar picks up is this counter current, and not the more prominent eastward current. It should be mentioned that the position of this radar could have been better - it reached only partway into the area of high regression factor as seen on Figure 4.6. This has, however, not disproved that there is a relationship between NAO and current speed in Skagerrak. It should also be mentioned that, since there were very few data points, daily values for current and NAO index were used. This is not ideal, since it is doubtful that the lag is so short between NAO and the current speed in Skagerrak. The NAO is considered a variation that spans longer time scales than daily. However, daily NAO data can be an indicator of whether the NAO is in a positive or negative phase. The analysis of observational data in general would also have benefited from having more locations and longer time series of data. However, data was sparse in the locations of interest, specifically in Skagerrak.

5.3 Limitations and Perspectives

This section will look into what could have been improved, what limitations there were, and what the future perspectives of the work are.

EOF analyses have some inherent limitations that arise from the fact that the modes of variability by definition are orthogonal in space and time. This means that there are no spatial correlations between two EOFs and also that no two PC time series have any simultaneous temporal correlation. This is not necessarily true in the natural world, making EOF analyses faulty in that sense. This can be partly avoided by using rotated EOF anlysis, which removes the spatial constraint of the EOF (Lian and Chen, 2012). Even if EOF analyses has these constraints, they are still useful in order to explain the main modes of variability. It was therefore deemed unnecessary to perform a rotated EOF analysis in this thesis.

When doing the comparison of the MSLP and oceanic variables PC time series, the correlations were mostly low, especially on the monthly timescales. However, the p-values were extremely small (for example e-30), meaning that the correlations were very significant, even though the correlations were quite low. This is not wrong in itself, but one should be careful using such low p-values to discard or confirm a hypothesis. An extremely small p-value indicates that the null hypothesis is incompatible with the data (Jung, 2017). It can be understood that "one asks the data the wrong questions". As mentioned earlier, it is expected that the p-values were that low because the correlations have been done without taking into account auto-correlation between the points. This would reduce the degrees of freedom drastically. Also, the act of varying the time lag to optimize the correlation will reduce the degrees of freedom. The p-values were more reasonable when it came to the extended winter data, since larger time averages reduce the degrees of freedom.

As mentioned in the Background, the ocean lags the atmosphere on timescales shorter than a decade, whereas it might be the other way around on longer time scales (Hurrell and Visbeck, 2003). Since only monthly, extended winter, and three year Gaussian smoothing timescales were used, it would be interesting analyse the lags further with longer time averages in order to see if the ocean indeed leads the NAO on decadal timescales. These multi-decadal responses between the NAO and the ocean are, however, controversial (Hurrell and Visbeck, 2003).

Most of the effects that the NAO has on oceanic variables discussed in this thesis, occur with an NAO in either a persistent positive or negative phase. A further point of analysis could be to filter out the data point where the NAO has not been exclusively in either a negative or positive phase. This would presumably reduce the noise of data greatly, since the noise arises when the system switches phase often.

An area of further research for this thesis would be, firstly, to establish to a higher level of precision how the NAO affects the current in Skagerrak. Secondly, one could look into proxy data from Skagerrak, for example isotope data, which then could be used for reconstructions of the NAO back in time. One of the goals in the GreenPlanning was to better the reconstruction of the NAO beyond just the NAO index. Looking into the conditions in Skagerrak could play into this.

Conclusion

This thesis successfully performed an EOF analysis on MSLP, SST, OHC, salinity, and current speed, identifying the first two modes of variability for each of the variables. The PCs from the EOF analyses were used to determine which patterns of variability co-varied with NAO, as well as determining a lag on monthly time scales between the oceanic variables that did co-vary with NAO. The EOF analysis results were further used in a PC regression analysis where the oceanic variables (raw data, not their EOFs) were regressed onto the EOF pattern which represented the NAO. This was done in order to determine the effect of the NAO on the variables.

In addition to this statistical analysis of the climatology in the NA region, a simple analysis was done with observational data of the volume transport across the GSR and eastward current speed measurements from Skagerrak. They were plotted against NAO index, and a linear trend was fitted.

These analyses were done in order to answer the questions; *How does the North Atlantic Oscillation influence oceanic variables in the North Atlantic?, Is it possible to identify a time lag between NAO phases and oceanic variables? and is it possible to see an effect of the North Atlantic Oscillation in oceanic observational data?*

The results from the PC time series comparisons determined that the NAO does co-vary with SST, OHC, and SSH, meaning that these patterns of variability are effected by each other. No co-variance between salinity and current speed from the PC time series comparison was found, therefore patterns of variability do not influence each other. This was due to the low explained variance of the current speed EOFs and the limited area analyzed for salinity..

It was found that the NAO leads the SST tripole by one month in the cross correlation analysis, This was in accordance with other studies. The NAO and SSH anomalies were found to have no lag, which is also in accordance

with other studies. However, it was discussed that the result might have been different if this was split up into smaller areas, since the response of SSH is normally quick on continental shelves, while one could expect some lag on the open ocean.

From the PC regressions it was found that SST varied ± 1 degrees Kelvin with the NAO loading, or in the case of OHC $\pm 8 * 10^8$ J/m^2, while the SSH varied with ± 0.1 m with NAO loading. This was in rough accordance with other studies.

The observational data from the FSC volume transport showed a small positive trend with NAO index. The regression coefficient is 0.41 m^{3}s^{-1} per "NAO index", while the r-squared value was 0.21. The other two currents, NIIC and the IF current, did not show an influence from the NAO. The observational data from Skagerrak showed a small westward trend with NAO index. This was due to a counter current positioned north of the strong eastward current that arose with NAO.

Since the current in Skagerrak is highly correlated the the NAO, an area of further research and an area of interest to the GreenPlanning project, would be to explore the conditions in Skagerrak. One of the goals of the GreenPlanning project is to better the reconstruction of the NAO beyond just the NAO index. Looking into the conditions in Skagerrak could play into this.

Bibliography 7

Bjornsson, H. and S. A. Venegas (1997). *A Manual for EOF and SVD Analyses of Climate Data*.

C3S (2023a). *ERA5 hourly data on single levels from 1959 to present*. URL: `https://cds.climate.copernicus.eu/cdsapp#!/dataset/reanalysis-era5-single-levels?tab=overview` (visited on Mar. 2, 2023).

C3S (2023b). *ORAS5 global ocean reanalysis monthly data from 1958 to present*. URL: `https://cds.climate.copernicus.eu/cdsapp#!/dataset/reanalysis-oras5?tab=overview` (visited on Mar. 2, 2023).

Enfield, David, Alberto Mestas-Nunez, and Paul Trimble (May 2001). „The Atlantic Multidecadal Oscillation and its relation to rainfall and river flows in the continental U.S." In: *Geophysical Research Letters - GEOPHYS RES LETT* 28.

Esselborn, Saskia and Carsten Eden (2001). „Sea surface height changes in the North Atlantic Ocean related to the North Atlantic Oscillation". In: *Geophysical Research Letters* 28.18, pp. 3473–3476. eprint: `https://agupubs.onlinelibrary.wiley.com/doi/pdf/10.1029/2001GL012863`.

Hughes, Chris W and Michael P Meredith (2006). „Coherent sea-level fluctuations along the global continental slope". In: *Philosophical Transactions of the Royal Society A: Mathematical, Physical and Engineering Sciences* 364.1841, pp. 885–901.

Hurrell, J and National Center for Atmospheric Research Staff (2021). *Hurrell North Atlantic Oscillation(NAO) Index(station-based)*.

Hurrell, James W., Yochanan Kushnir, Geir Ottersen, and Martin Visbeck (2003). „An Overview of the North Atlantic Oscillation". In: *The North Atlantic Oscillation: Climatic Significance and Environmental Impact*. American Geophysical Union (AGU), pp. 1–35. eprint: `https://agupubs-onlinelibrary-wiley-com.ep.fjernadgang.kb.dk/doi/pdf/10.1029/134GM01`.

Hurrell, James W. and Martin Visbeck (2003). „The Ocean's Respons to North Atlantic Oscillation Variability". In: *The North Atlantic Oscillation: Climatic*

significance and environmental impact. American Geophysical Union, pp. 113–141.

Iglesias, Isabel, M Nieves Lorenzo, Clara Lázaro, M Joana Fernandes, and Luisa Bastos (2017). „Sea level anomaly in the North Atlantic and seas around Europe: Long-term variability and response to North Atlantic teleconnection patterns". In: *Science of the Total Environment* 609, pp. 861–874.

Jung, Inkyung (2017). „Some facts that you might be unaware of about the p-value". In: *Archives of Plastic Surgery* 44.02, pp. 93–94.

Lian, Tao and Dake Chen (2012). „An evaluation of rotated EOF analysis and its application to tropical Pacific SST variability". In: *Journal of Climate* 25.15, pp. 5361–5373.

Lutgens, Frederick K, Edward J Tarbuck, and Dennis Tusa (1995). In: *The atmosphere*. Prentice-Hall Englewood Cliffs, NJ, USA. Chap. Chapter 7: Circulation of the Atmosphere.

Martinson, Douglas G. (2018). „15 - Empirical Orthogonal Function (EOF) Analysis". In: *Quantitative methods of data analysis for the Physical Sciences and Engineering*. Cambridge University Press, pp. 495–534.

Masson-Delmotte, VP, P Zhai, SL Pirani, C Connors, S Péan, N Berger, Y Caud, L Chen, MI Goldfarb, and Pedro M Scheel Monteiro (2021). „Ipcc, 2021: Summary for policymakers. in: Climate change 2021: The physical science basis. contribution of working group i to the sixth assessment report of the intergovernmental panel on climate change". In.

North, Gerald R, Thomas L Bell, Robert F Cahalan, and Fanthune J Moeng (1982). „Sampling errors in the estimation of empirical orthogonal functions". In: *Monthly weather review* 110.7, pp. 699–706.

Pan, Lin-Lin (2005). „Observed positive feedback between the NAO and the North Atlantic SSTA tripole". In: *Geophysical Research Letters* 32.6.

Rahmstorf, Stefan (1997). „Risk of sea-change in the Atlantic". eng. In: *Nature (London)* 388.6645, pp. 825–826.

Sarafanov, Artem (2009). „On the effect of the North Atlantic Oscillation on temperature and salinity of the subpolar North Atlantic intermediate and deep waters". In: *ICES Journal of Marine Science* 66.7, pp. 1448–1454.

Schulzweida, Uwe (Oct. 2022). *CDO User Guide*. Version 2.1.0.

Taylor, Arnold H and John A Stephens (1998). „The North Atlantic oscillation and the latitude of the Gulf Stream". In: *Tellus A: Dynamic Meteorology and Oceanography* 50.1, pp. 134–142.

Toma, Vincenzo de, Vincenzo Artale, and Chunxue Yang (2022). „Exploring AMOC Regime Change over the Past Four Decades through Ocean Reanalyses". In: *Climate* 10.4, p. 59.

Trenberth, K, R Zhang, and National Center for Atmospheric Research Staff (2019). *The Climate Data Guide: Atlantic Multi-decadal Oscillation (AMO)*.

Volkov, Denis L. and Hendrik M. van Aken (2003). „Annual and interannual variability of sea level in the northern North Atlantic Ocean". In: *Journal of Geophysical Research: Oceans* 108.C6. eprint: `https://agupubs.onlinelibrary.wiley.com/doi/pdf/10.1029/2002JC001459`.

Wanner, Heinz, Stefan Brönnimann, Carlo Casty, Dimitrios Gyalistras, Jürg Luterbacher, Christoph Schmutz, David B Stephenson, and Eleni Xoplaki (2001). „North Atlantic Oscillation–concepts and studies". In: *Surveys in geophysics* 22, pp. 321–381.

Appendix

8.1 Mean fields of the variables

The mean fields of the oceanic variables in the time period 1959-2022.

(a) Mean field of SST

(b) Mean field of OHC

(c) Mean field of current speed

(d) Mean field of salinity
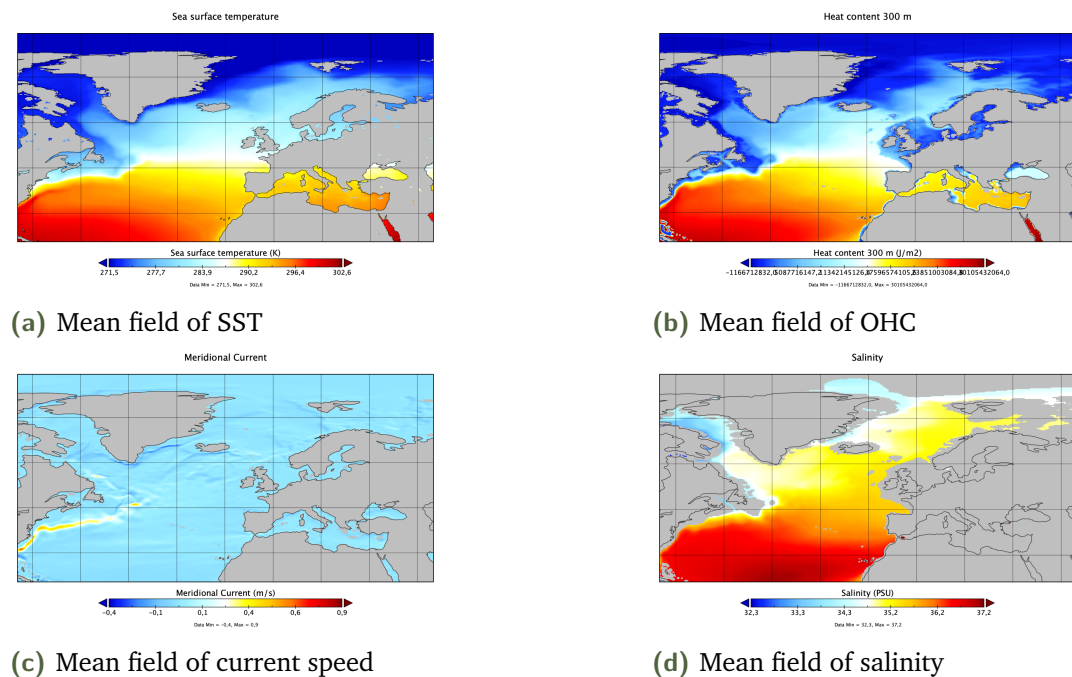
Figure 8.1: The mean fields of the oceanic variables. Notice that it it says meridional current, but this is in fact the meridional and zonal components combined

8.2 Eigenvalue spectrums for monthly means
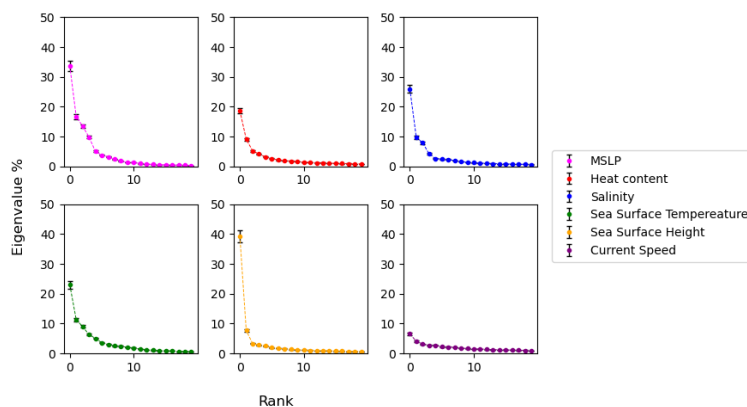
Figure 8.2: Eigenvalue spectrum for each of the variables considered using monthly means. The explained variance of the 20 first leading EOFs including associated errors

8.3 EOF analysis of Salinity

(a) Monthly EOF patterns of Salinity

(b) monthly PC time series

(c) Yearly EOF patterns of Salinity

(d) Yearly PC time series
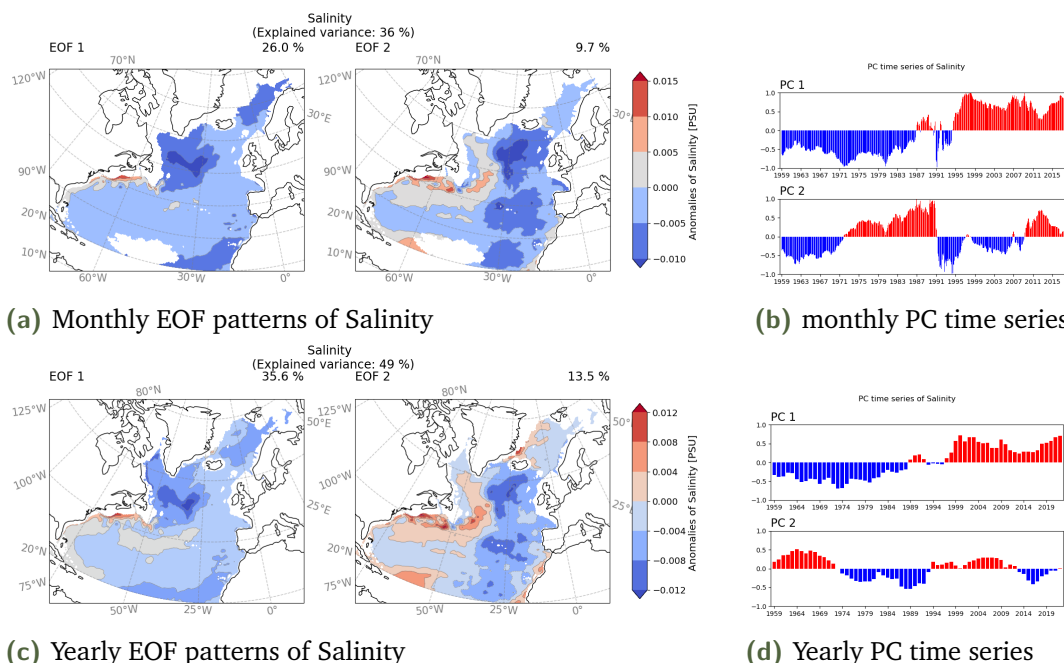
Figure 8.3: The result of the EOF analysis of Salinity. (a), (c): the patterns of the two leading modes of variability for Salinity based on monthly and yearly means respectively. (b), (d): the corresponding PC time series of the two leading modes of variability on based on monthly and yearly means respectively.

8.4 EOF analysis of Current speed

(a) Monthly EOF patterns of Current Speed

(b) monthly PC time series

(c) Yearly EOF patterns of Current Speed

(d) Yearly PC time series
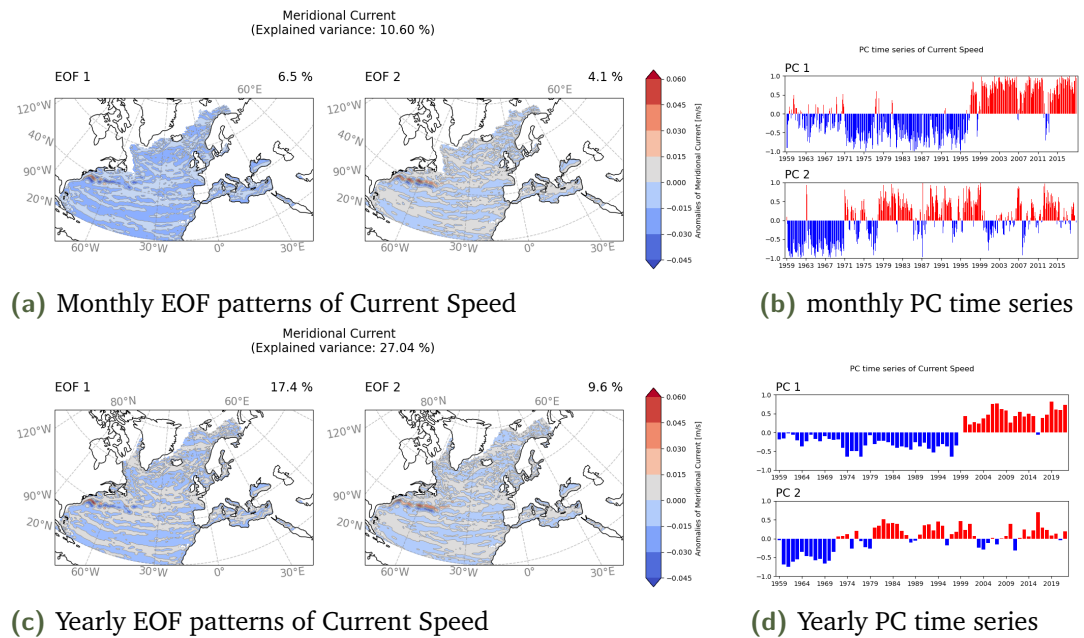
Figure 8.4: The result of the EOF analysis of Current Speed. (a), (c): the patterns of the two leading modes of variability for Salinity based on monthly and yearly means respectively. (b), (d): the corresponding PC time series of the two leading modes of variability on based on monthly and yearly means respectively.

8.5 EOF analysis of detrended SST and OHC

(a) Monthly EOF patterns of detrended SST

(b) monthly PC time series

(c) Seasonal EOF patterns of detrended SST

(d) seasonal PC time series
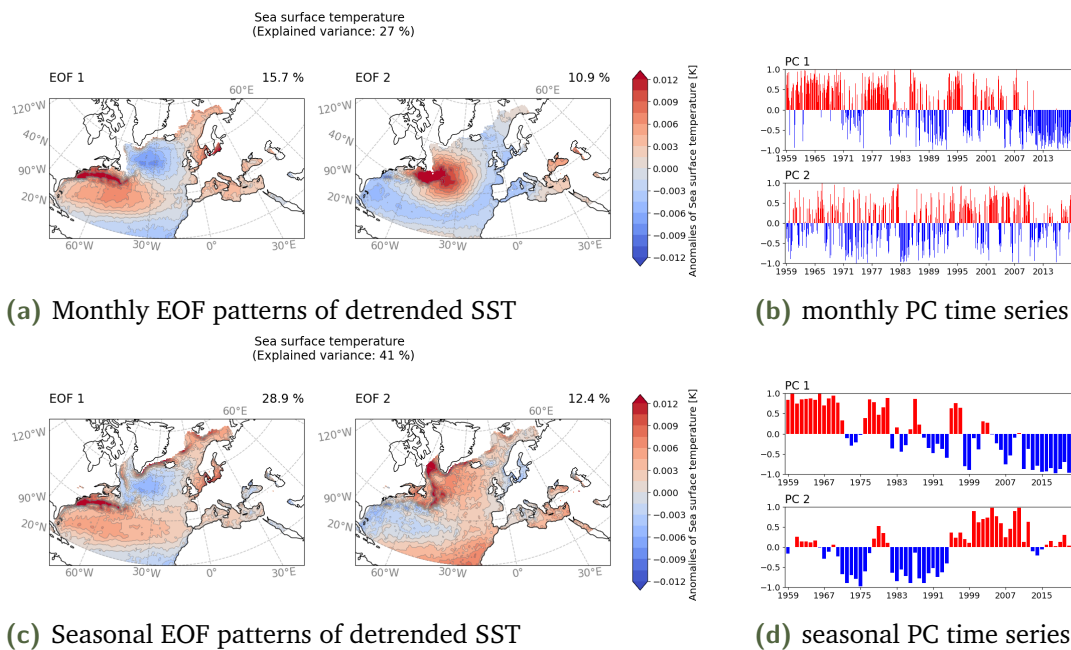
Figure 8.5: The result of the EOF analysis of detrended SST. (a), (c): the patterns of the two leading modes of variability for SST based on monthly and seasonal(DJFMA) means respectively. (b), (d): the corresponding PC time series of the two leading modes of variability on based on monthly and seasonal means respectively.

(a) Monthly EOF patterns of detrended OHC

(b) monthly PC time series

(c) Seasonal EOF patterns of detrended OHC

(d) seasonal PC time series
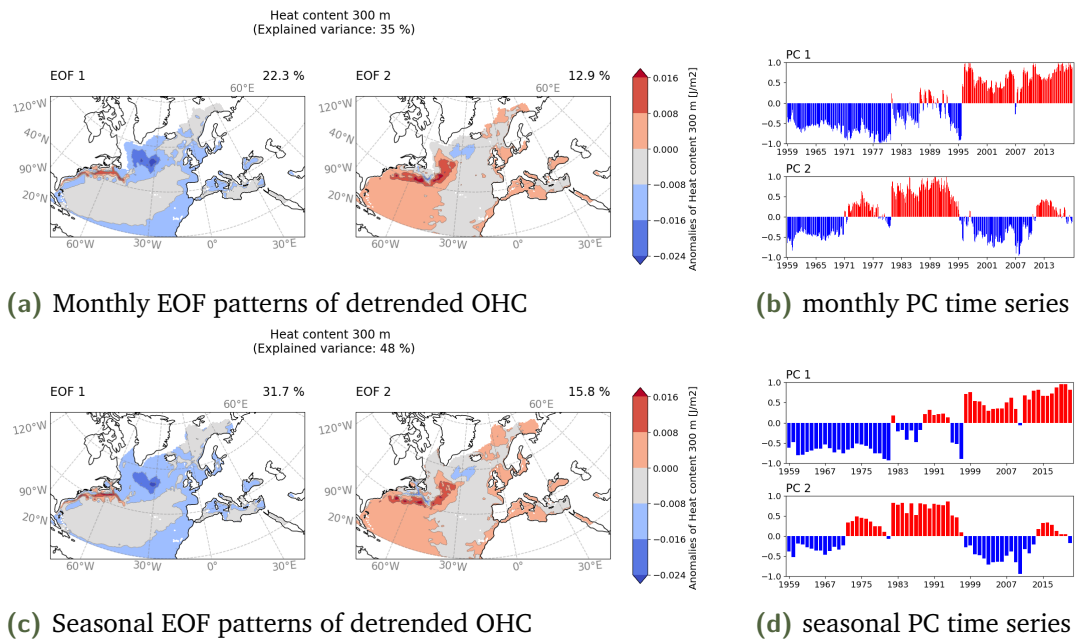
Figure 8.6: The result of the EOF analysis of detrended OHC. (a), (c): the patterns of the two leading modes of variability for OHC based on monthly and seasonal(DJFMA) means respectively. (b), (d): the corresponding PC time series of the two leading modes of variability on based on monthly and seasonal means respectively.

8.6 Detrended PCs cross correlation
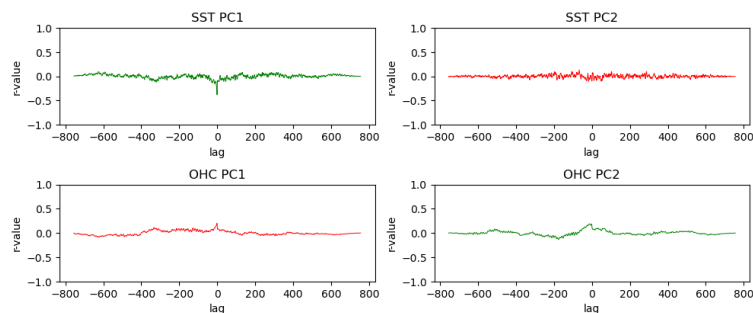
Figure 8.7: The cross correlated lags between detrended SST and Heat content and MSLP.

8.7 Correlation maps
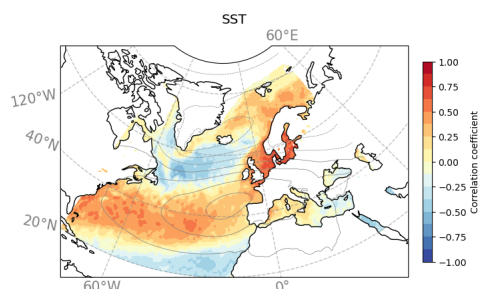
(a) Correlation between SST and the leading mode of MSLP
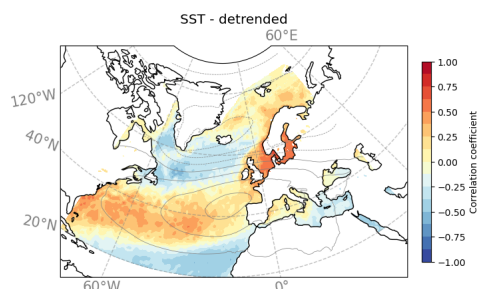
(b) Correlation between detrended SST and the leading mode of MSLP
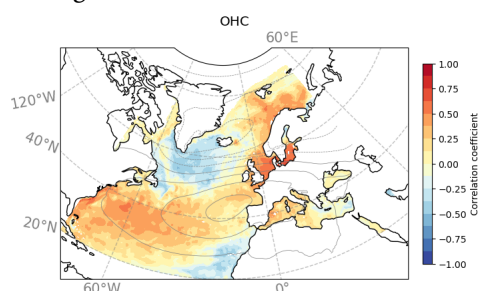
(c) Correlation between OHC and the leading mode of MSLP
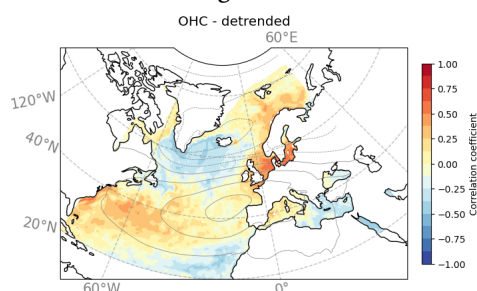
(d) Correlation between detrended OHC and the leading mode of MSLP
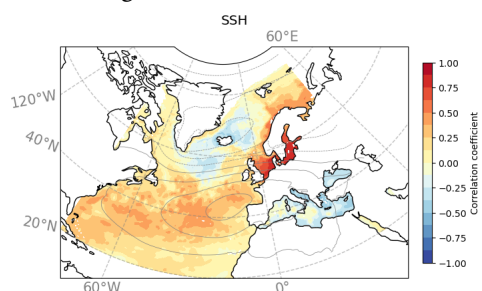
(e) Correlation between SSH and the leading mode of MSLP
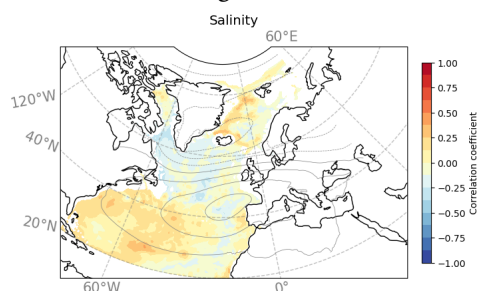
(f) Correlation between Salinity and the leading mode of MSLP
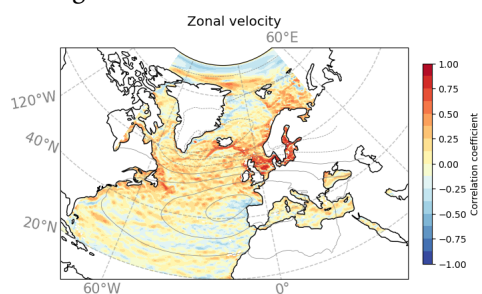
(g) Correlation between Zonal velocity and the leading mode of MSLP
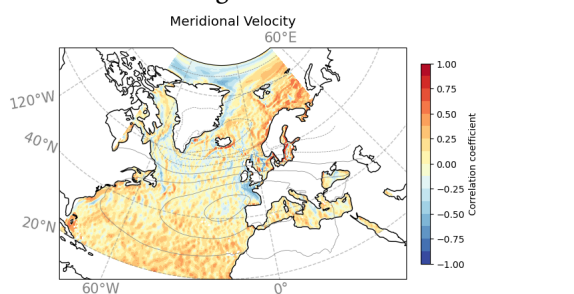
(h) Correlation between Meridional velocity and the leading mode of MSLP

Figure 8.8: Correlation maps between all variables individually and the first mode of MSLP, the NAO

8.8 Unmasked PC regressions

(a) PC regression between SST and the leading mode of MSLP

(b) PC regression between detrended SST and the leading mode of MSLP

(c) PC regression between OHC and the leading mode of MSLP

(d) PC regression between detrended OHC and the leading mode of MSLP

(e) PC regression between SSH and the leading mode of MSLP

(f) PC regression between Salinity and the leading mode of MSLP

(g) PC regression between Zonal velocity and the leading mode of MSLP

(h) PC regression between Meridional velocity and the leading mode of MSLP

Figure 8.9: PC regression maps between all variables individually and the first mode of MSLP, the NAO